Article

Sensitivity of Flood Hazard and Damage to Modelling Approaches

Charlotte E. Lyddon [1,2,*], **Jennifer M. Brown [2]**, **Nicoletta Leonardi [1]** and **Andrew J. Plater [1]**

[1] School of Environmental Sciences, University of Liverpool, Liverpool L69 7ZT, UK; N.Leonardi@liverpool.ac.uk (N.L.); gg07@liverpool.ac.uk (A.J.P.)

[2] National Oceanography Centre Liverpool, Joseph Proudman Building, 6 Brownlow Street, Liverpool L3 5DA, UK; jebro@noc.ac.uk

* Correspondence: c.e.lyddon@liverpool.ac.uk

check for updates

Abstract: Combination of uncertainties in water level and wave height predictions for extreme storms can result in unacceptable levels of error, rendering flood hazard assessment frameworks less useful. A 2D inundation model, LISFLOOD-FP, was used to quantify sensitivity of flooding to uncertainty in coastal hazard conditions and method used to force the coastal boundary of the model. It is shown that flood inundation is more sensitive to small changes in coastal hazard conditions due to the setup of the regional model, than the approach used to apply these conditions as boundary forcing. Once the threshold for flooding is exceeded, a few centimetres increase in combined water level and wave height increases both the inundation and consequent damage costs. Improved quantification of uncertainty in inundation assessments can aid long-term coastal flood hazard mitigation and adaptation strategies, to increase confidence in knowledge of how coastlines will respond to future changes in sea-level.

1. Introduction

The combined effect of astronomical high tides, storm surges, wind and waves during hurricanes and violent storms can temporarily increase sea level at the coast to exceed critical hazard thresholds, and lead to flooding, damage to infrastructure and potential loss of life. This is particularly critical in heavily populated, industrialised estuaries and deltas, which are the focal point of coastal megacities and hubs for transport, trade and critical infrastructures [1–3]. The concurrence or close succession of different sources of flood hazard, defined as compound hazards [4], can generate disproportionately large and adverse consequences for estuaries with a macro- and hyper-tidal regime. Even small changes in water level can influence wetting and drying, local fetch, wave and surge propagation, wave runup, refraction and dissipation to elevate flood hazards at the coast [5].

It is of critical, international importance that we fully understand the sources, pathways and degree of exposure of flood hazard in estuaries [6]. The following events show how high tides, storm surges, wind and waves can combine in macro- and hyper-tidal estuaries to elevate flood and wave hazard. The combined effect of strong winds, high tides and low atmospheric pressure has caused substantial damage on the coastline of the Bay of Fundy, Canada; 166 km/h winds from a category 2 hurricane caused a 2 m storm surge on a spring tide and subsequent overtopping of dykes by 0.9 m to cause damage to buildings, railroads and livestock during the Saxby Gale on October 4–5 1869 [7]. The Groundhog Day storm on 2 February 1976 saw wind speeds exceed 164 km/h and a 2.1 m storm surge caused up to 1.6 m flooding in coastal towns including Saint John, New Brunswick,

as towns were left without power for 14 days [8]. A perigee new moon spring tide, combined with a 989 mb low pressure system and 6 m waves at Bristol Channel buoy caused one of the worst winter storms in the UK on 3 January 2014; many defences held but some flooding occurred across low-lying agricultural land on the Somerset Levels [9,10]. Typhoon Hato caused 12 fatalities and up to USD 4.34 billion of flood damage in the city of Macau on the south coastline of the Pearl River Estuary on 23 August 2017, as observed tides were 6.14 m above predicted level; a 2.79 m meteorological storm surge was exacerbated by 127.9 km/h winds generating large wind setup [11].

An understanding of the nature and degrees of exposure to coastal flood hazard from extreme storms and hurricanes is important for reducing its impacts on communities, property and infrastructure. There is a need for accurate predictive techniques, visualisation tools, vulnerability maps, timely flood alerts and warning systems to mitigate the negative consequences of hazards. It is particularly important to mitigate the negative consequences of combined hazards in estuaries as it has been shown that these extreme events present a threat to life [12]. These mitigation techniques require an accurate understanding of the hydrodynamic processes in estuaries during hurricanes and violent storms, and an understanding of coastal and estuarine response to hydrodynamic forcing [13,14]. The accurate prediction of sources of flood hazard during storms, water level (WL) and significant wave height (H_s), most notably at the time of high water when defence exceedance is most likely to occur, is an important component of flood hazard management, due to their influence on wave runup, wave overwashing and erosion [5,15,16]. Hydrodynamic numerical modelling tools are widely used to predict high water level (HWL) and wave parameters, for example high water significant wave height (HWH_s) in coastal and estuarine regions. Outputs from numerical modelling tools can be used to design crest levels of flood defence structures [17], or force the model boundary of process-based and shoreline response models to predict the pathway, maximum velocities and extent of floodwater, and timing of peak discharge, [18–20], wave overtopping [21], morphological change [22,23] and hazard rating [24] arising from the combined effect of these hazards. However, uncertainty can arise in modelled HWL and HWH_s predictions due to bathymetric and topographic resolution [25] model coupling processes, local forcing processes and coastal geometry [26]. Therefore an additional key component of flood hazard assessment is to identify sources of uncertainty in HWL and HWH_s predictions, and the main objective of this study is to quantify how these uncertainties can propagate through the modelling chain from regional models to generate uncertainty in the impacts of flooding events simulated by process-based and shoreline response models.

Uncertainty refers here to a lack of sureness about a specific parameter, e.g., HWL or HWH_s, where a range of possible values may exist for a single variable within which exposure or impacts could occur [27], and can occur due to misrepresentation of physical processes in numerical models [28]. Inaccurate representation of the complex interactions between atmospheric, meteorological, fluvial and tidal processes in estuaries can propagate through the modelling chain and result in large uncertainties in the hydrodynamic forcing of process-based and shoreline response models [29], and have been shown to cause uncertainties in subsequent model outputs. The exclusion of locally generated winds underestimated HWH_s by up to 90.1% in the upper regions of the Severn Estuary, southwest England, during simulations of the 3 January 2014 storm event [26]. Excluding the contribution of riverine discharge to total water level during simulations of a storm-tide, using hydrodynamic modeling package Delft3D, underestimates flood extent by 30% (20.5 km^2) in the Shoalhaven Estuary, south-eastern Australia [30]. LISFLOOD-FP, a 2D inundation model, has been used to show that uncertainties in boundary conditions are an important factor in the accurate prediction of inundation of the coastal city of Licata, in the Imera basin, Sicily, as this determines whether or not rivers are in flood and reach bankfull stage and discharge [31]. LISFLOOD-FP has also been used to show the differential flood risk from different combinations of storm return period, wave overtopping and river discharge in Fleetwood, northwest England, and quantified economic impact [19]. LISFLOOD-FP has also been used to assess the sensitivity of future coastal flooding in the Severn Estuary, given uncertainty over possible mean sea-level rise and storm surge climate [32–34]. Accurate estimation of still water-level,

wave setup and runup is crucial for accurate representation of peak storm tides, and may be more important in a coastal inundation model than intra-modeling uncertainties, such as bed roughness coefficients and input conditions [34]. There is a need to accurately predict HWL and HWH_s for flood hazard management and quantify uncertainties in hydrodynamic models due to the parameterisation and interaction of physical processes when used to force process-based and shoreline response models, for example inundation or hydro-morphological models.

The impacts and relative importance of the sources of uncertainty in hydrodynamic models on model outputs can be assessed using sensitivity analysis. Sensitivity analysis is used here to achieve the main objective of the research to quantify the sensitivity of inundation to uncertainty in HWL and HWH_s. This is a common approach to explore and quantify the impacts of uncertainty by determining the change in a result arising from a specific variation in input values or assumptions [28]. Systematically varying model setup or boundary conditions can help to understand the relative importance of individual contributions of uncertainty and assess the impact of uncertainty on the spatial and temporal variability of coastal hazards [35]. Sensitivity analysis can be undertaken on model calibration parameters (e.g., Manning's *n*), wind effects, boundary flows and discharge levels, or initial water levels [36]. This approach can also be used to quantify the sensitivity of inundation assessments to conceptual schemes used to assign probabilities to hazard magnitudes [37]. Input parameters are adjusted within plausible limits, and the impact on response quantified; greater variability in model outputs indicates sensitivity to a certain model setup or variable, and this input is identified as generating a larger degree of uncertainty [38], and efforts can then be directed to reduce uncertainty, or account for it in future decisions. Decisions in flood hazard assessments need to minimise damage and loss of life, and there is a need to understand uncertainty in the data which supports these assessments to minimise confusion, delay, or potential errors in decisions. The more that is known about uncertainties, via sensitivity analysis, then the more confidence decision makers can have in future plans or strategies. Therefore, there is a pressing need to understand how uncertainties in coastal hydrodynamic models propagate and accumulate through the modeling chain to influence process-based and shoreline response models, and the accuracy of their outputs for practical, hazard assessment purposes in large, developed estuaries.

Case Study

This research aims to understand how uncertainty in the sources of coastal hazards (HWL and HWH_s) propagates through the modelling chain to impact flood hazard at Oldbury-on-Severn on the south coastline of the Severn Estuary, southwest England (Figure 1). The Severn Estuary can be defined as hyper-tidal and has a tidal range up to 12.2 m at Avonmouth as the tide is funnelled up-estuary. The most extreme event on record, 3 January 2014, generated a 0.48 m skew surge on a 10.01 m tide and had a return period of 20 years [39,40]. Large local fetch at high tide means southwest-west wind direction can generate and propagate locally generated waves up-estuary to Oldbury [26]. Historically, Oldbury and the low-lying area of Oldbury Naite has been susceptible to coastal flooding due to the combined effect of tide-surge-wind-wave-river hazards [41]. Flood hazard occurs here due to the combined effect of HWL, H_s and winds resulting in the overwashing of lowered foreshore levels and defences as greenwater [18,42], rather than wave overtopping which causes dense, vertical plumes of water to travel over the crest. Further to this, inundation occurs in these low-lying areas of the Severn Estuary due to overflow from tidal inlets and channels, breaching of defences and embankments [43], and high estuary and sea water levels causing tide locking [44]. The study area extends from the Severn Bridge to the west, up to Sharpness harbour to the east. Land use is predominantly rural as well as some urban areas close to the coast, including Berkeley-on-Severn (population 2034) and Oldbury-on-Severn (population 780) [45]. Low-lying agricultural areas at Oldbury Naite, local transport networks and towns are afforded a level of protection from coastal hazards by 9.0 to 9.5 m OD earthen banks along the south coastline of the estuary [18]. A decommissioned nuclear facility at Oldbury, named Oldbury

Technical Centre, is protected by earthen banks and concrete seawall, with a tidal pool extending 825 m from the coastline into the estuary.
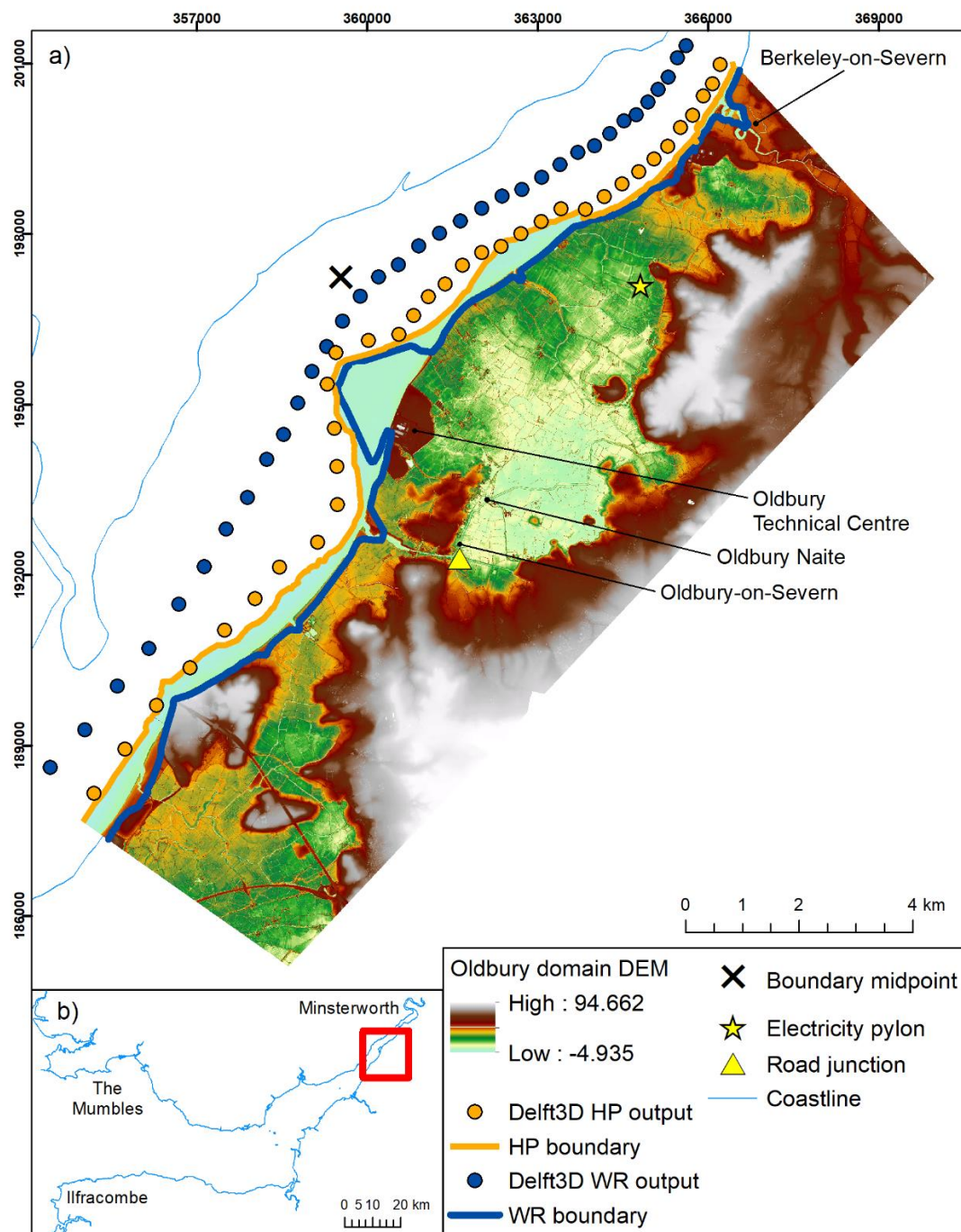

Figure 1. (**a**) Oldbury model domain, including the location of Delft3D outputs (coloured dots) used to force the hazard proxy (HP) and wave runup (WR) boundary approach (coloured lines); boundary midpoint to calculate change in coastal hazard uncertainty (black cross); sites of critical infrastructure (yellow star and triangle); and (**b**) Delft3D model domain with extent of the up-estuary Oldbury model domain shown.

Section 2 of this paper will discuss the inundation model, input data and inundation scenarios completed for two historic storm events. Section 3 presents flood maps to systematically show the maximum depth and extent of inundation for each scenario and presents flood hazard ratings at sites

of critical infrastructure. The sensitivity of time-integrated volume of inundation and economic cost of damage of each scenario to uncertainty in regional model predictions of WL and H_s is quantified. Before drawing conclusions in Section 5, Section 4 will discuss the sensitivity of depth, extent and volume of inundation across the model domain to uncertainty in boundary conditions and position, and local coastal morphology, and how even small changes in HWL and HWH_s at the boundary have a significant impact on coastal flood hazard.

2. Method

Figure 2 shows the model inputs and processes followed to derive the impact of each inundation scenario, which are explained through Section 2.
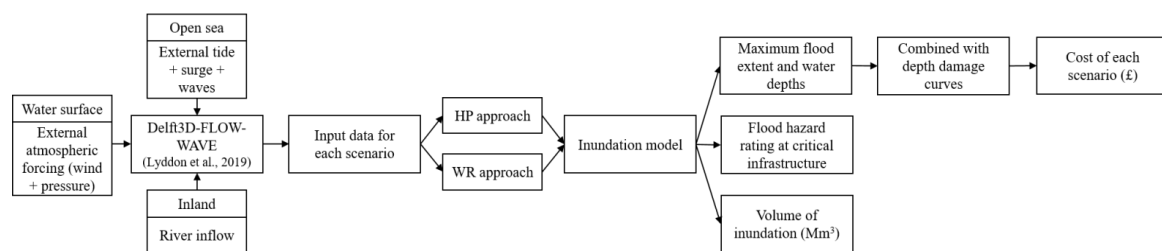

Figure 2. Model inputs and the process followed to propagate and quantify uncertainty in flood hazard assessments, and results that are presented in Section 3.

2.1. Inundation Model

LISFLOOD-FP [46] is used to quantify the sensitivity of inundation to coastal hazard uncertainty and approach to forcing the model boundary influences the impacts at an up-estuary location. LISFLOOD-FP is a 2D finite difference inundation model based upon the storage cell approach [46]. The model simulates the movement of water across a grid representing the bathymetry and land surface, based on LiDAR data, under the influence of gravity. The model has been successfully used in other coastal applications to replicate tidal elevations and wetting and drying, and simulate inundation during storm events in the Solent [47], Humber Estuary [48], and the Severn Estuary [34,49,50]. The DEM used for the Oldbury model domain were obtained from EA Geomatics [51], and the data have a 1 m horizontal resolution and 0.05 m to 0.15 m vertical accuracy. Uncertainty in the vertical accuracy of the DEM can arise due to equipment and methods used in obtaining the topographic data, and may influence the representation of energy loss and flood wave propagation through the model domain and, hence, predicted floodwater routing, depths and extents [52–54]. The DEM was resampled to 5 m horizontal resolution to ensure computational efficiency. The model domain is 17 km in length, and up to 6.5 km wide. Defences, including earthen banks, are well represented at 5 m in the model domain. Inland river channels, known locally as rhines and pills, were digitised into the DEM to ensure accurate representation of the floodplain. Topographical features, such as bridges, were removed as these can act as artificial dams. The acceleration solver is used in this study, which assumes only the convective acceleration term is negligible and implements adaptive time steps.

2.2. Input Data

2.2.1. Historic Storm Events

The Delft3D modeling system has been previously validated and successfully used to simulate coastal hazards in the Severn Estuary for two historic storm events; (i) 3 January 2014 (hereafter called January 14) which represents the maximum coastal hazard condition; and (ii) 16 December 2012 (hereafter called December 12) which represents the 90th percentile coastal hazard condition, represented by WL + $\frac{1}{2}$ H_s [26]. These storm events coincide with winds from a southwest-west direction at the time of high water, as wave hazard is amplified up-estuary with winds from this

direction [26]. Flood warnings were issued along large stretches of the Oldbury coastline for the 3 January 2014 storm event, and flooding was reported 10 km further up-estuary locations in the Severn Estuary at Minsterworth as defences were overwashed [39].

2.2.2. Coastal Hazard Uncertainty

Coastal hazard uncertainty at the boundary of LISFLOOD-FP is approximated by a sensitivity analysis from eight model simulations (Table 1) completed for the January 2014 and December 2012 events in Delft3D across the entire Severn Estuary model domain (Figure 1b). The Delft3D model for the Severn Estuary uses a two-dimensional, horizontal curvilinear grid which has been previously validated and successfully used in [5,25]. Each model simulation was forced with a combination of time-varying, spatially uniform WL from Ilfracombe tide gauge and time-varying, space-varying H_s from the UK Met Office WAVEWATCH III hindcast [55,56] at the open sea boundary representing different model coupling setups. A time-varying, spatially uniform WL boundary is a common approach, and small changes (<0.15 m) in WL are observed across the open boundary. WL outputs have been well validated at up-estuary locations, which shows that small changes in WL across the open sea boundary are not propagated up-estuary and are unlikely to impact the floodplain model.

Table 1. Eight model simulations completed in Delft3D for each historic storm event, and outputs used to force the boundary of the Oldbury model domain in LISFLOOD-FP from the low water mark and defence crest. Run 8 has been successfully validated to tide gauges and wave buoys throughout the model domain and is used as the baseline scenario.

Run	Model	Coupling	Forcing
1	FLOW	Standalone	Water level
2	FLOW	Standalone	Water level + wind
3	WAVE	Standalone	Constant total water level + Wave
4	WAVE	Standalone	Constant total water level + Wave + wind
5	FLOW WAVE	One-way	Water level from 1 + wave
6	FLOW WAVE	One-way	Water level from 1 + wave + wind
7	FLOW WAVE	Two-way	Water level + wave
8	FLOW WAVE	Two-way	Water level + wave + wind

Uncoupled model scenarios represent standalone water level simulations in FLOW, which use a time-varying, spatially uniform WL boundary, or wave simulations in WAVE, which superimpose time- and spatially-varying H_s on a constant total water level at mean high water spring tide, taken from Ilfracombe tide gauge. Mean high water spring tide represents a HWL which could present a hazard to coastal zones. One-way coupled scenarios represent the influence of currents on waves, and two-way scenarios represent the influence of currents on waves, and waves on currents. Simulations were forced with and without local wind conditions, originating from the Met Office global unified model [57] and extracted from the Extended Area Continental Shelf Model CS3X [58] to represent changing forcing processes. All simulations were forced with river gauge data from the Environment Agency Sandhurst river gauge near Gloucester at the eastern open boundary. Run 8 represents a complete, 5-parameter multi-hazard simulation and outputs were graphically and statistically validated to tide gauges and wave buoys in the estuary [5,26]. The results of the Delft3D runs were used to force the boundary of the LISFLOOD-FP Oldbury model domains to represent coastal hazard uncertainty.

2.3. Inundation Model Boundary Conditions

LISFLOOD-FP can be forced with a water level or discharge at its open boundaries. We tested two approaches to forcing the model boundary (as indicated in Figure 1a) to represent different methodologies for determining the pathway of flood hazard (described in Sections 2.2.1 and 2.2.2).

1. Hazard proxy (HP = WL + $\frac{1}{2}$ H_s) is calculated from Delft3D outputs and imposed at the low water mark, to resolve wetting and drying in the inundation model.
2. WL and H_s from further offshore are used to calculate wave runup using Stockdon formula [59], and provide runup level at the crest.

For both approaches to forcing the model boundary the time- and space-varying predicted WL and H_s from the eight Delft3D model simulations (see Table 1), representing coastal hazard uncertainty, were used. The position of the model boundary is different for both approaches, represented by the blue line in Figure 1 for the WR approach applied at the defence crest, and orange line for the HP approach applied at the low water mark. Apart from the position of the model boundary, the resolution and extent of the grid is the same.

2.3.1. Hazard Proxy Approach

The first approach to forcing the LISFLOOD-FP model boundary uses HP imposed at the low water mark. This method assumes that waves do not break before the defence crest and regards combined WL+Hs as still water to exceed the defence crest level.

WL and H_s outputs from the Delft3D Severn Estuary model domain were extracted from the Delft3D grid cell closest to the low water mark boundary of the Oldbury model domain (see Figure 3). LISFLOOD was forced with WL only from the Delft3D outputs of run 1 and 2, constant HWL + $\frac{1}{2}$ H_s from run 3 and 4, and HP was calculated for run 5, 6, 7, and 8 along the boundary of the Oldbury model domain.
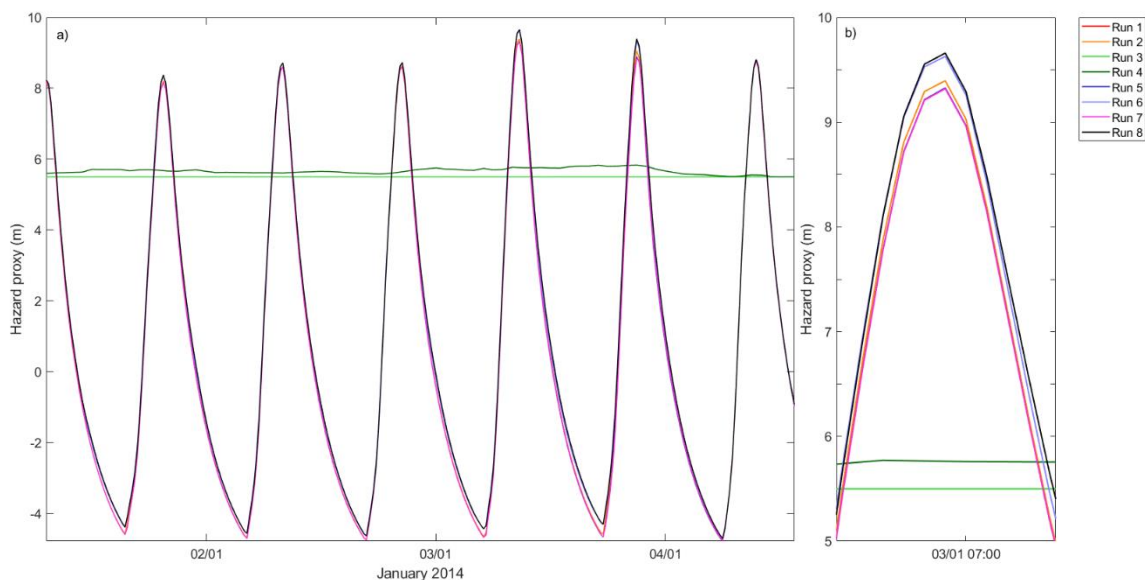

Figure 3. (**a**) Coastal hazard uncertainty time series from Delft3D used to force LISFLOOD-FP, for January 14 event using the HP approach, shown here as an example; (**b**) zoom of peak of the January 14 event to show coastal hazard uncertainty.

2.3.2. Wave Runup Approach

The second approach to forcing the boundary combines maximum wave runup (WR), which determines the extent of which waves act [60], with water level to determine flood inundation

from the effect of overwashing at the defence. The 2% exceedance runup level was calculated from Stockdon formula [59];

$$R_2 = 1.1 \left(0.35 \, \beta \left(H_s L_p \right)^{0.5} + \frac{H_s L_p \left(0.563 \, \beta^2 + 0.004 \right)^{0.5}}{2} \right) \tag{1}$$

where β represents the slope angle of earthen embankments along the coastline, calculated in ArcMap from the DEM, H_s represents significant wave height in the thalweg of the estuary, and L_p represents wavelength, calculated as;

$$L_p = \frac{gT^2}{2\pi} \tag{2}$$

where T represents peak wave period. H_s and L were extracted from the Delft3D domain from the deepest part on the Severn Estuary channel. WR was calculated and added to Delft3D water level outputs at the coastline, extracted from the second grid cell into the domain along the coastline. Total water level at the time of the storm tide peak, at the boundary midpoint (see Figure 1) is calculated for January 14 as 9.69 m (HWL: 9.4 m, WR: 0.29 m) and December 12 is 8.17 m (HWL: 8.03 m, WR: 0.14 m). As seen in Figure 1, the LISFLOOD-FP boundary is forced from the defence crest of the earthen embankments along the south coastline of the Severn Estuary, to represent flood hazard due to overwashing of greenwater from waves and water level.

2.4. Model Validation and Calibration

Qualitative comparison of flood extents between secondary sources and outputs from run 8 were undertaken for the January 14 event. Evidence of flooding is documented in the Severn Estuary during this event on SurgeWatch [39,40], due to overtopping and overwashing of banks. The event has a return period of 1 in 20 years down estuary at Ilfracombe, indicating this storm has a 5% chance of occurring in any given year [39], but this might be different at an up-estuary location. The Severn Estuary Shoreline Management Plan (SMP) shows similar extent of inundation for a 1 in 20 year storm event occurring in 2008 when compared to inundation simulated by run 8 using the WR approach [61]. These flood zones are probabilistic and linked to return period, so are not directly comparable with the real, percentile events simulated here; however, they can be useful to show which areas are in a flood hazard zone. The SMP shows defence breaches occur east of Oldbury Technical Centre and low-lying agricultural land behind the defences and near tidal inlets are flooded. Inundation for a 1 in 50 year event in the SMP also shows similar extents of inundation near Avonmouth and Berkeley for run 8 for the HP approach, which could be accurate if the return period at Oldbury-on-Severn is different to the one calculate for Ilfracombe. Environment Agency inundation maps show that areas inundated by run 8 at Oldbury-on-Severn, Oldbury Naite and Berkeley-on-Severn are all in flood zone 3, indicating greater than 0.5% probability of inundation from tidal flooding, and greater than 1% probability of river flooding [62]. Further to this, large areas of Oldbury-on-Severn are shown to be vulnerable to a 1 in 100 year event, and local weak points in defences at Berkeley-on-Severn means there is a 10% probability of tidal flooding on agricultural land [63]. The areas inundated in run 8 are like those shown in the SMP flood maps and known to be vulnerable to flood hazard, indicating the LISFLOOD-FP model setup can be used to simulate flooding with confidence.

Qualitative comparison with secondary sources also informed calibration of the Manning's friction coefficient, which controls flow resistance and energy loss and hence, floodwater propagation. A uniform Manning friction coefficient is used throughout the floodplain, based on the recommendation of Chow tables [64,65] for a grassy floodplain with minimal crops and minor obstructions, and those used in similar studies [66–68]. A series of sensitivity tests were conducted for values between 0.018–0.6 during the most extreme event on record (3 January 2014). A value of 0.03 was selected as this generated inundation most similar to flood zones in the SMP [10]. A time- and space-varying Manning friction

coefficient could reduce errors in modelled inundation; however, this is dependent on data availability and increases computational time.

2.5. Flood Inundation Scenarios

LISFLOOD is run for 32 simulations in total (eight coastal hazard uncertainty scenarios, for two approaches to forcing the model boundary, for two historic events). The inundation model was run from 48 h before the selected storm event to allow spin up, to 12 h after the event. The coastal hazard conditions that occur at the time of the storm tide peak for the January 14 and December 12 events are the conditions of interest in this study. This study aims to simulate inundation that occurs due to these coastal hazards condition at the storm tide peak, so the simulation is run to 12 h after the peak of the selected storm tide.

Outputs presented in Section 3 assess and quantify the sensitivity of inundation to coastal hazard uncertainty and approach to forcing the model boundary. Impact proxies include inundation maps showing maximum depth and extent of inundation are analysed systematically for all scenarios. Results are then presented from low water to low water over the tidal cycle of each extreme event. Flood hazard rating [69] is calculated for two locations of critical infrastructure within the Oldbury model domain to show degree of flooding at a road junction on Oldbury Naite rhine (51.63° N, −2.56° W) and an electricity pylon between Oldbury Technical Centre and Berkeley (51.64° N, −2.55° W). Flood hazard rating is calculated at each location as:

$$Flood\ hazard\ rating\ =\ water\ depth\ \times\ (floodwater\ velocity + 0.5) \tag{3}$$

where 0.5 represents a constant value [24]. Flood hazard rating is presented at each site of critical infrastructure relative to thresholds to hazard to people. A flood hazard rating of 0.75–1.25 indicates hazard to some (e.g., children), 1.25–2.0 represents hazard to most, and over 2.0 represents hazard to all, including emergency responders [24].

The volume of inundation in the model domain is presented in million cubic metres (Mm^3), and then absolute difference in time-integrated volume of inundation (m^2/s) and economic cost of inundation to suburban and arable land is calculated. This is presented against absolute difference in HP at the boundary midpoint at the time of HW for each run to show how an increase in regional model WL and H_s changes flood hazard. Run 8 is used as a baseline to quantify absolute difference; each absolute difference value indicates what the change in HP, time-integrated volume of inundation or economic cost of inundation is from each model run relative to the value simulated for run 8 (i.e., a positive value of 0.2 m difference in HP indicates run 8 is 0.2 m larger than the model run). Absolute difference is calculated for each variable (e.g., volume of inundation, hazard proxy at the boundary midpoint, economic cost of inundation) from each model run to model run 8 is calculated as:

$$Absolute\ difference\ =\ variable\ ^{Run\ 8}\ -\ variable^{Run\ X} \tag{4}$$

where *X* indicates outputs from simulations 1–7 shown in Table 1.

2.6. Depth Damage Curves

The depth and extent of floodwater at the time of maximum inundation in model cells with depth greater than 0.05 m are combined with saltwater depth damage curves [70] to place an economic value on each scenario. Water depths less than 0.05 m are considered not damaging and are below the vertical accuracy of the LiDAR data [19]. Land-use was classified using the 25 m UK Land Cover 2015 dataset [71], and combined with depth damage curves depending on the land use. The impact of inundation on arable land use is based on uniform costs per m^2 that is inundated (Table 2).

Table 2. Arable Damage Costs (£) per Inundated Cell [56].

Arable Damage Costs	
Land Use	**Cost per m^2 (£)**
Arable and Horticulture	0.57
Improved Grassland	0.09
Rough Grassland	0.025
Neutral Grassland	0.05

Damage for suburban land uses was classified using a saltwater depth damage curve for housing (Table 3). Urban and arable damage was calculated for each scenario and is presented as percent difference compared to run 8.

Table 3. Saltwater Depth Damage (£) for Urban Flood Inundation Cells [56].

Urban Damage Curve	
Depth (m)	**Cost per m^2 (£)**
0	0
0.05	663
0.1	1822
0.2	2224
0.3	2705
0.6	2935
0.9	3217
1.2	3477
1.5	3774
1.8	4026
2.1	4265
2.4	4819
2.7	5062
3	5062

3. Results

The outputs from each simulation, detailed in Table 1, have been displayed over Ordnance Survey 1:250,000 (Ordnance Survey, 2019) scale map to highlight infrastructure and communities impacted by inundation. Figures 4 and 5 show the flood at its maximum extent during the 3 January 14 event. The flood maps show water depths above 0.05 m, which is the depth saltwater inundation is considered damaging, and is standardised up to the average 99th percentile water depth for run 8 of the coastal hazard condition (2.7 m for January 14) to more clearly present inundation with shallower depths. The 90th, 50th and 10th percentile water depths are quoted in the text as indicators of the proportion of the flooded areas during the maximum extent and the extent of shallow water inundation which could cause impacts within the model domain. All water percentile depths for all model simulations are provided in Supplementary Information 1. Flood inundation maps are presented in Supplementary Information 2 for the December 12 event.

3.1. Depth and Extent of Inundation

3.1.1. January 14 Hazard Proxy (HP)

Figure 4 shows the sensitivity of the maximum depth and extent of flood inundation to coastal hazard uncertainty for January 14 using the HP approach (WL + $\frac{1}{2}$ H_s). Run 3 and 4 flood only the tidal inlets at Oldury Naite and Berkeley, as constant water level at MHWS + H_s does not exceed the bank crest and floodwater does not breach channels. Excluding run 3 and 4, as the model scenarios become more realistic (from run 1 to run 8), inundation becomes increasingly widespread in the southwest of the model domain, near Oldbury-on-Severn and Littleton-upon-Severn, and is focused around tidal inlets and rhines which have been exceeded. Low-lying agricultural areas in the centre of the model domain near Oldbury Naite see increasing extent of inundation from run 2, 6 to 8, up to 1 m deep. Runs which do not include locally generated winds in the boundary condition for LISFLOOD-FP (run 1, 5 and 7) do not cause inundation in these central areas of the model domain because peak HP at the time of HW is lower. Berkeley, to the northeast of the model domain, is inundated as Berkeley Pill is exceeded in all scenarios, and water depths of over 1 m occur to the east of the channel.

Run 8 represents the greatest extent of inundation, with a 90th percentile water depth of 1.29 m, which shows 10% of the area of inundation exceeds this depth, notably away from full or deep channels e.g., local, man-made channels which flow between agricultural and pastoral fields called rhines and pills. Run 6 shows a similar extent of inundation, and 90th percentile water depth of 1.3 m. Run 8 and 6 have a 50th percentile water depth of 0.47 and 0.49 m, and a 10th percentile water depth of 0.14 m. The 10th percentile water depth indicates that 10% of inundation occurs below this depth. These shallower depths of inundation may cause saltwater damage to roads, housing and agricultural land. Run 2 has a 90th percentile water depth of 1.3 m, similar to run 8, but lower 50th (0.36 m) and 10th (0.07 m) percentile water depths. This indicates that water depths across much of the model domain are shallower than 0.36 m. Run 2, 6 and 8 all include local atmospheric forcing in the boundary condition. Inclusion of locally generated wind causes greater flooding by increasing the peak HP value, and makes the HP peak wider to allow higher and longer inflows. Run 1, 5 and 7 show smaller extent of flood inundation than run 2, 6 and 8, and also lower 50th water depth percentiles between 0.35–0.37 m, indicating the majority of floodwater is shallower. The results presented here signify that coastal hazard uncertainty influences the depth and extent of inundation.
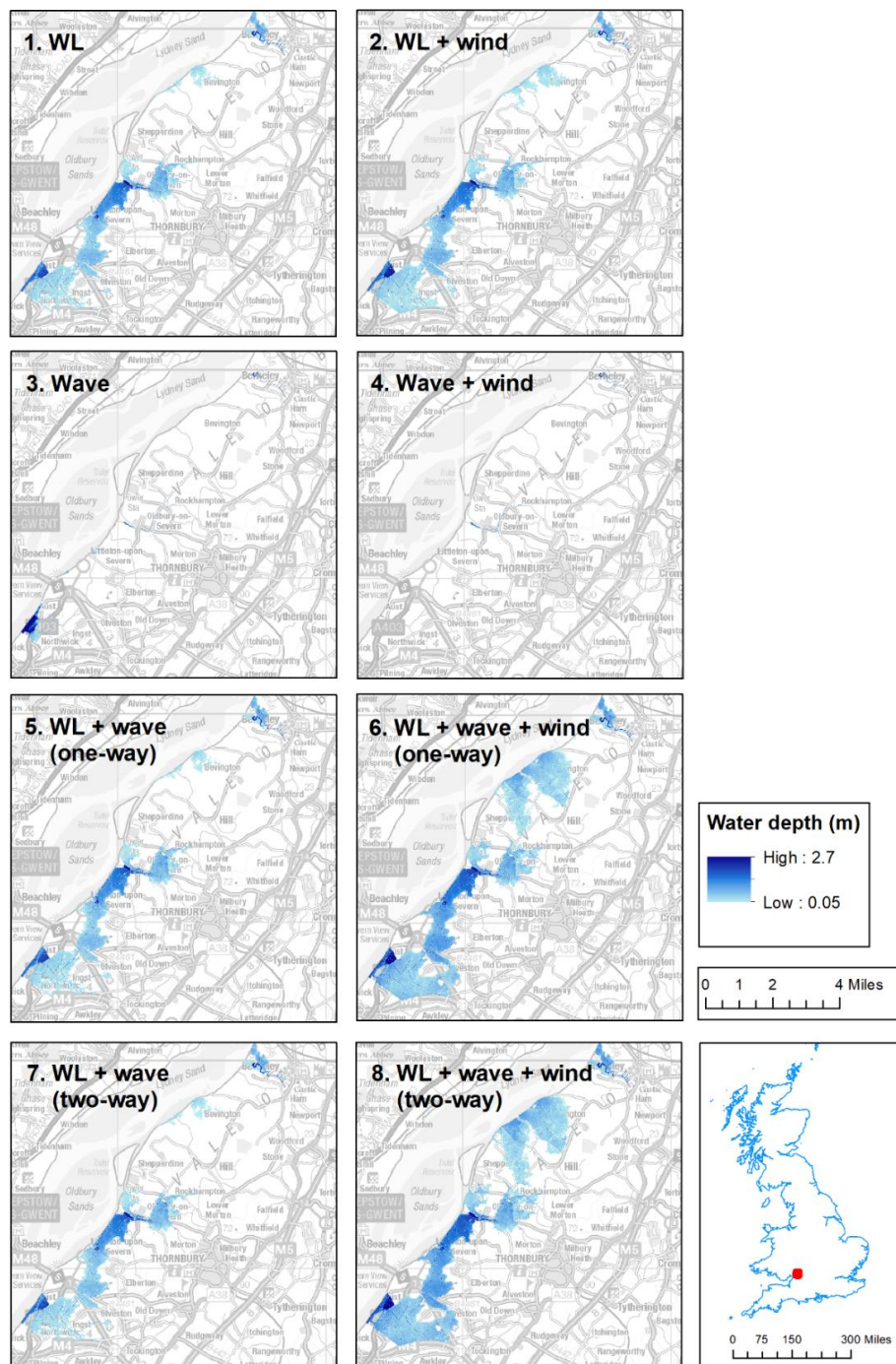
Figure 4. Depth and extent of flooding at Oldbury-on-Severn for HP approach to forcing the model boundary where maps 1–8 represent coastal hazard uncertainty (see Table 1) for January 14.

3.1.2. January 14 Wave Runup (WR)

Figure 5 shows the maximum depth and extent of flood inundation for January 14 using the wave runup approach. Inundation is widespread in the northeast of the model domain for all runs, south of Berkeley-on-Severn (excluding run 3 and 4, which show no inundation when using the WR approach). Steeper earthen embankments along the coastline in the northeast of the model domain and large HWH$_s$ during the January 14 event means overwashing occurs at multiple locations. Inundation in the southwest of the model domain, near Littleton-upon-Severn and Severn Beach, becomes increasingly

widespread from run 1 to run 8. Less inundation is seen around Oldbury Naite rhine. The pattern of inundation seen here can be described as being opposite to what occurs when using the HP approach.

Run 8 shows the greatest extent and depth of inundation, with a 90th percentile water depth up to 1.38 m, and a 50th percentile water depth up to 0.7 m, which is up to 0.23 m larger than the HP approach. Run 6 shows a similar extent and a 50th percentile water depth of 0.62 m. The 10th percentile water depth is 0.21 m and is larger than the HP approach, indicating that 90% of inundation in the model domain is deeper than 0.21 m. Run 1, 5 and 7 show smaller extent and depths than run 6 and 8, with 50th percentile water depths of 0.45 m, and 10th percentile water depths of 0.1 m.
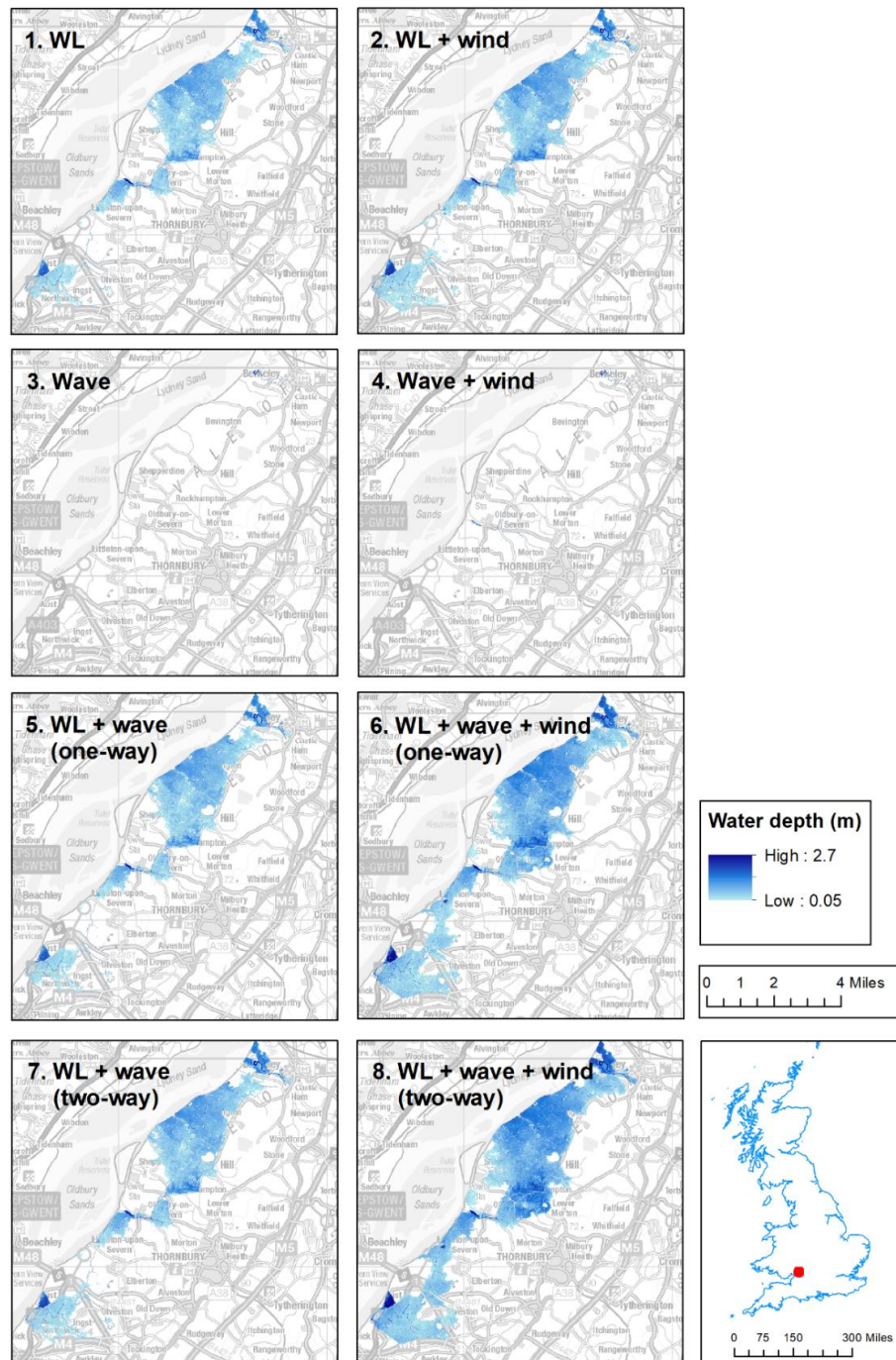

Figure 5. Depth and extent of flooding at Oldbury-on-Severn for WR approach to forcing the model boundary where maps 1–8 represent coastal hazard uncertainty (see Table 1) for January 14.

Figures 4 and 5 illustrate that a more complex mode setup causes the greater extent of inundation overall during the January 14 event. Inundation from the low water mark occurs in the southwest and northeast of the model domain where rhines and pills are exceeded. Inundation from the defence crest occurs where defences are steeper and lower, increasing maximum WR to cause overwashing at multiple locations along the central coastline of the domain. Inundation is sensitive to coastal hazard conditions, as inundation is more widespread and deeper for simulations which include local atmospheric forcing. Inundation also shows sensitivity to approach to forcing the model boundary and event severity; January 14 shows greater depth of shallow water inundation using WR approach. Run 3 and 4 show minimal inundation as they are forced with a constant water level, and inundation is focused around rhines and mudflats when it does occur.

3.2. Flood Hazard Rating at Operational Sites

Flood hazard rating, calculated using Equation (3), is shown at two sites of critical infrastructure at Oldbury; a road junction on Oldbury Naite rhine and an electricity pylon between Oldbury Technical Centre and Berkeley (locations shown in Figure 1a). Thresholds for flood hazard rating, which are related to hazard to people, are shown as horizontal coloured lines (moderate, significant, extreme) in Figure 6, to indicate the extent and duration of exceedance, and timing relative to HW, which is crucial information for emergency response planning.
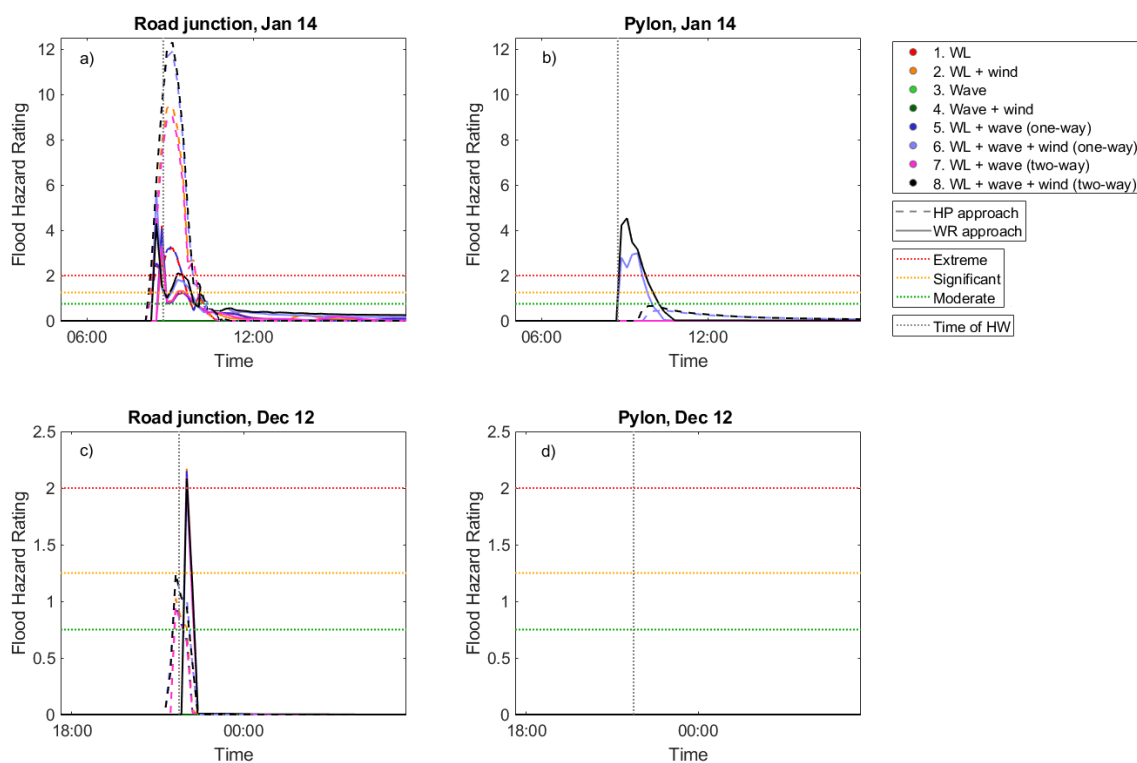

Figure 6. Flood hazard rating during the January 14 event at (**a**) road junction; (**b**) pylon; and during December 12 event at (**c**) road junction; and (**d**) pylon using the HP (dashed black line) and WR approach (solid black line). Modelled tidal signal at the boundary midpoint (vertical dotted black line) and extreme (red, horizontal dotted line), significant (amber, horizontal dotted line) and moderate (green, horizontal dotted line) thresholds for hazard to people [24].

Figure 6a shows flood hazard rating for January 14 at the road junction, where the greatest hazard occurs for run 8 from the HP approach, due to the combined effect of deeper water depths and increased floodwater velocities. Run 8, 7, 6, 5 and 2 show a rapid increase in hazard which exceeds the moderate threshold, indicating danger to some (i.e., children) 30 min before HW. The extreme

threshold, which indicates a flood zone with deep or fast flowing water and danger to all, is exceeded 25 min before HW, and peaks 23 min after HW at 09:05 a.m. Run 8 exceeds the extreme threshold for 1 h 39 min, and exceeds the moderate threshold for 2 h 13 min in total. The junction, at Pickedmoor Lane, Kington Road, Chapel Road and The Naite provide access routes from the M5 motorway to Oldbury Technical Centre and Oldbury-on-Severn. Access routes for emergency services would be shut for the duration of exceedance of the moderate threshold, and represents hazard to all, which may include children and vulnerable adults living nearby. The flood hazard time series curves show sensitivity to changes in coastal hazard uncertainty and approach to forcing the model boundary. A range of flood hazard rating values are seen for the same event in Figure 6a which cross all thresholds, indicating that for the same event there may be a danger to none or to all. Footpaths, conveniences (pub, shop, hotel) and a primary school located near flooded areas, such as the road junction may or may not be at risk of flooding and damage during the event, making it difficult to know if or when to issue warnings or evacuation notices. Sensitivity in hazard time series curves is also seen on the December 12; however, there is a narrower spread of results, as run 8 and 6 exceed the extreme threshold for just 4 min, and the moderate threshold is exceeded for 23 min. There is a smaller danger to all during the less extreme event.

Figure 6b shows flood hazard rating for January 14 at the pylon. Run 8 and 6 (Figure 6b) exceed all thresholds when using the WR approach, representing a danger to some and to all. The moderate threshold is exceeded for up to 1 h 53 min, and the extreme threshold is exceeded for 1 h 4 min. When using the WR approach, run 8 and 6 represents 1 h 53 min that the pylon would not be accessible; however, the moderate threshold is not exceeded when using the HP approach, indicating that the pylon would be accessible. Sensitivity in the hazard time series curves for run 8 and 6 covers all thresholds, meaning emergency planning is difficult; a flood event could mean the pylon is or is not accessible.

3.3. Volume of Inundation in the Model Domain

Figure 7 shows the change in volume of inland inundation from LW to LW for the January 14 and December 12 event. The more extreme coastal hazard condition generates a greater volume of flood water, as WL and H_s increase height and duration of peak HP and WR at the boundary. The largest volume of flood water for January 14 is generated by run 8 using the WR approach, which is 12.5 Mm^3. More inundation occurs for January 14 using the WR approach as it has larger H_s (0.58 m) and longer peak wave period (3.1 s) at peak of the storm tide for run 8, compared to December 12 (H_s: 0.3 m, peak wave period: 2.7 s). Larger H_s and longer peak wave period generate higher WR values, with differences being more significant on steeper slopes. Conversely, the largest volume of flood water for the December 12 event is generated by run 6 using the HP approach (see Figure 7), which is 5.6 Mm^3.
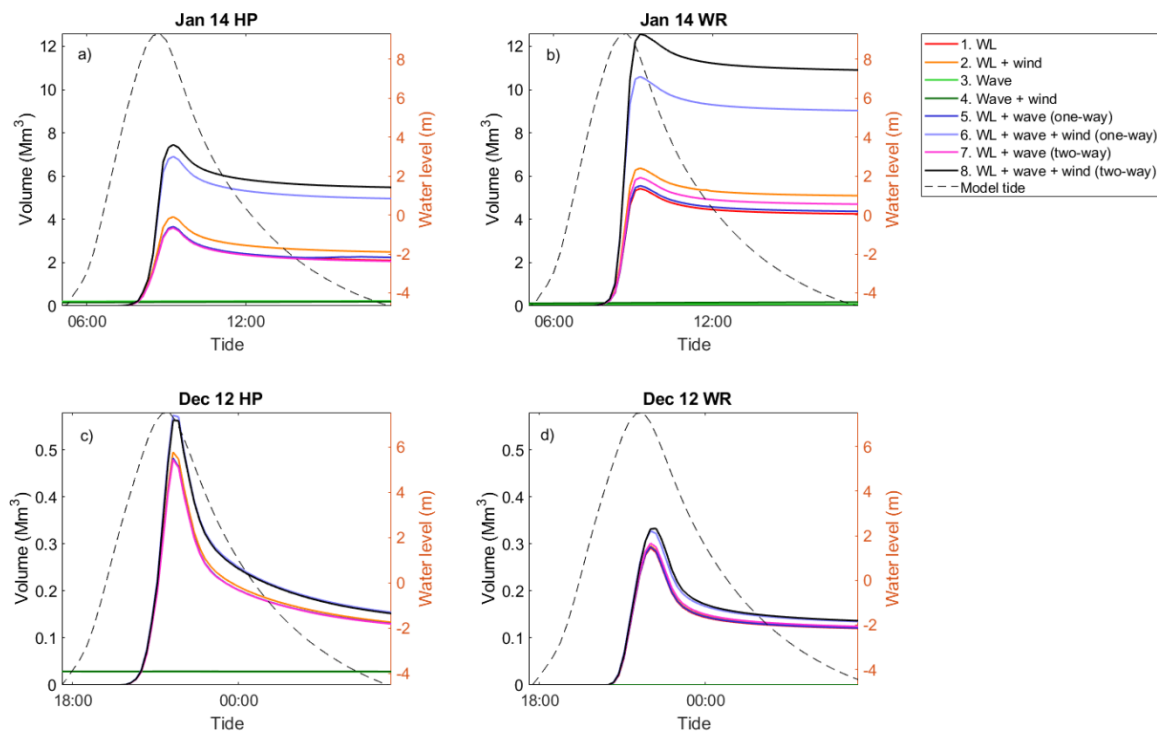
Figure 7. Change in volume of inundation (Mm³) in the Oldbury model domain for January 14 forced by (**a**) HP and (**b**) WR; and December 12 forced by (**c**) HP and (**d**) WR. Modelled high tide from low water to low water is also shown (dashed line).

The January 14 event shows greater sensitivity to coastal hazard uncertainty. Run 8 and 6 show greatest volumes of flood water, and then run 1, 2, 7 and 5 are grouped together, with run 1 generating 7.1 Mm³ less flood water than run 8 using the WR approach. Run 3 and 4 show minimal volumes of flood water in the model domains. The results of the December 12 event are similarly grouped, but show smaller differences between them, with run 1 generating just 0.05 Mm³ less flood water than run 8 when using the WR approach.

Both events show rapid inundation, and maximum volume of flood water occurs at the same time for each event, with a lag of 8 min after tidal high water, which may also be a function of the time step selected for the model simulation. Both events show asymmetric drainage from the model domain. Drainage of floodwater after the time of high water is most rapid for the December 12 event using the HP approach, and volume of inundation continues to fall for the duration of the ebb tide. Floodwater recedes slowly on the ebb tide and drainage plateaus when using the WR approach, which may be a result of the control hinterland topography has on the spread of the hazard across the model domain.

3.4. Flood Hazard Sensitivity to Coastal Hazard Uncertainty

Figure 8 shows sensitivity in flood hazard (represented by differences in volume of floodwater inundation in the model domain) due to coastal hazard uncertainty. The difference in time-integrated volume of inundation between HP and WR approaches are compared to difference in HP between each Delft3D run with run 8 at the boundary midpoint (black cross in Figure 1a). This value is the same for the WR and HP approach as the same dataset is used to generate the boundary conditions. The difference in HP is calculated as the change in WL + $\frac{1}{2}$ Hs at the time of high water between each run and run 8, which is used here as a baseline and simulation which generated maximum flood volume, at a point mid-domain alongshore to show how an increase in regional model WL and H_s changes flood hazard. The difference in time-integrated volume of inundation is calculated by integrating over the x-axis in Figure 7, by using the trapezium method to calculated area under the volume curves between each run and run 8, divided by total time (duration of inundation). Units are

given in million cubic metres/second (Mm^3/s). All results present positive difference; this signifies an increase in value presented from each run to run 8. The change in symbol colour in Figure 8 indicates a different run; change in symbol shape indicates coastal hazard condition (January 14 or December 12 event); unfilled symbols represent the WR approach to forcing the model boundary and filled symbols represent the HP approach. Lines connect same runs for each approach to forcing the model boundary for each coastal hazard condition.
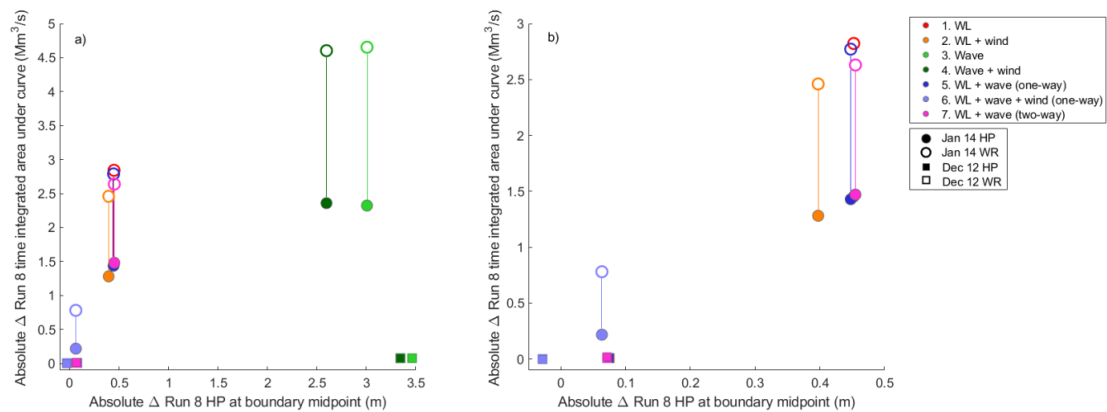

Figure 8. Absolute difference in HP at the boundary midpoint (shown in Figure 1a) against absolute difference in time-integrated volume for (**a**) all runs compared to baseline run 8 for each WR or HP simulation, depending on the approach used to force the model boundary.; and (**b**) zoomed into run 1, 2, 5, 6, and 7.

Figure 8a shows that there is substantial difference in HP at the boundary midpoint (location shown in Figure 1a and time-integrated volume of inundation between run 3 and 4 with run 8 for the January 14 (green circles). Coastal hazard uncertainty generates up to 3.46 m difference in HP at the boundary midpoint between run 3 and 8 for December 12, and 3 m for January 14.

Run 3 and 4 for January 14 shows greatest sensitivity to approach to forcing the model boundary. The WR approach generates up to 4.7 Mm^3/s difference in inundation between run 3 and 8, and 4.6 Mm^3/s difference between run 4 and 8. Run 3 generates a 2.33 Mm^3/s difference in time-integrated volume of inundation in the model domain between WR and HP approaches.

December 12 generates just 0.08 Mm^3/s differences in volume of inundation between run 3 and 8, and shows smaller sensitivity to approach to boundary forcing with a difference of 0.0006 Mm^3/s between WR and HP. Runs 3 and 4 are outliers, and not realistic as they are forced with a constant water level; total water level is greatly underestimated when tide is not included as a physical forcing process at the boundary.

Figure 8a shows results for realistic runs 1, 2, 5, 6 and 7, compared to run 8. Run 1, 5 and 7 are clustered together for the January 14 event, and sensitivity to approach to forcing the model boundary. The January 14 event shows up to 2.82 Mm^3/s difference in volume of inundation with 5.3% (0.45 m) difference in HP at the boundary midpoint, when forced using WR for run 1. The December 12 event shows substantially smaller difference in time-integrated volume of inundation. Run 7 generates 0.016 Mm^3/s difference in inundation with 0.07 m difference in HP, when forced using HP for run 7. The large difference in volumes of inundation generated between different runs for the January 14 and December 12 event indicates sensitivity to coastal hazard uncertainty. Run 1, 5 and 7 exclude local atmospheric forcing in the boundary condition, which means peak HP and WR values are lower and less overwashing of defences and embankments occurs in the Oldbury model domain. This indicates that the inclusion of local atmospheric forcing in boundary conditions is more important to reduce uncertainty in simulated inundation, than model coupling processes.

Run 2 (orange) is positioned on its own in Figure 8b for the January 14 event, and shows smaller uncertainty in HP at the boundary midpoint. Run 2 includes local atmospheric forcing,

which contributes towards to the peak of WR and HP but excludes wave contribution. This indicates model coupling processes are important to help to improve accuracy of prediction of coastal hazard conditions, but not as important as local atmospheric forcing.

Run 6 for January 14 shows smaller sensitivity in HP at the boundary midpoint, but sensitivity to approach to forcing the model boundary remains. For the maximum event, 0.06 m difference in HP at the boundary midpoint generates up to 0.78 Mm^3/s difference in time-integrated volume (purple, unfilled circle) using the WR approach. The inclusion of local atmospheric forcing and one-way coupling in the boundary forcing from Delft3D causes smaller sensitivity in HP at the boundary midpoint. Even a small change in HP at the boundary midpoint can mean hazard thresholds are exceeded to have a substantial impact on volume of inundation.

Overall, the more extreme coastal hazard condition (January 14) generates a steeper trend. January 14 shows increased sensitivity in flood hazard with increased uncertainty in coastal hazard uncertainty, and sensitivity to approach to forcing the model boundary. December 12 generates small volumes of inundation as thresholds for flooding are not exceeded.

3.5. Economic Cost of Inundation for Arable and Suburban Land Uses

Tables 4 and 5 show economic cost of inundation at the time of maximum inundation for arable and suburban land uses. Run 8 for January 14 using the WR approach generates greatest cost to arable land (£4.3 M) and to suburban land uses (£60.9 M). Runs 3 and 4 generate smallest economic cost at the time of maximum inundation, for both events across both model domains.

Table 4. Simulated Economic Cost of Inundation for Arable Land Cover.

Inundation Scenario		Arable Land Damage (£M)							
		1	2	3	4	5	6	7	8
January 14	HP	1.55	1.91	0.07	0.01	1.56	2.96	1.51	3.06
	WR	2.80	3.09	0.00	0.01	2.84	4.00	2.95	4.31
December 12	HP	0.07	0.07	0.01	0.01	0.07	0.10	0.07	0.10
	WR	0.02	0.02	0.00	0.00	0.02	0.03	0.02	0.04

Table 5. Simulated Economic Cost of Inundation for Suburban Land Cover.

Inundation Scenario		Suburban Land Damage (£M)							
		1	2	3	4	5	6	7	8
January 14	HP	44.85	46.48	6.13	2.46	44.89	53.10	44.71	54.35
	WR	33.01	36.06	0.62	2.45	33.48	48.55	34.73	60.91
December 12	HP	17.61	17.99	1.82	1.80	17.61	19.89	17.56	19.75
	WR	8.49	8.78	0.00	0.00	8.66	10.16	9.05	10.41

Figure 9 shows the absolute difference in HP at the boundary midpoint against absolute difference in economic cost to (i) arable land and (ii) suburban land at time of maximum inundation against each run and run 8. The economic cost of flood events is important information for shoreline management planning. The change in symbol colour in Figure 9 indicates a different run; change in symbol shape indicates coastal hazard condition (January 14 or December 12 event); unfilled symbols represent the WR approach to forcing the model boundary and filled symbols represent the HP approach. Lines connect same runs for each approach to forcing the model boundary for each coastal hazard condition. In the text absolute changes are shown below in brackets for context. Run 3 and 4 are not shown in the following analysis, as they are outliers and not realistic.
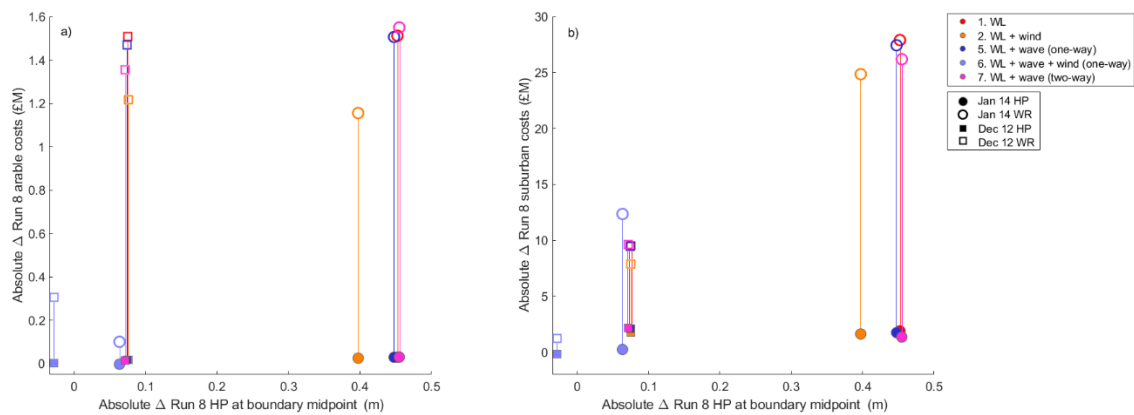
Figure 9. Absolute difference in HP at the boundary midpoint (shown in Figure 1a) against absolute difference in (**a**) arable land costs and (**b**) suburban land cost for runs 1,2,5,6 and 7 compared to baseline run 8 for each WR or HP simulation, depending on the approach used to force the model boundary.

Figure 9a shows absolute difference HP at the boundary midpoint and arable costs compared to run 8. As also seen in Figure 8 for the January 14 event, run 1, 5 and 7 are grouped for each event, and then run 2 is positioned on its own, with run 6 showing smallest uncertainty in HP and arable costs. Run 7 for the January 14 event with WR approach (unfilled, pink circle) generates up to £1.5M difference in arable costs, against 0.45 m difference in HP at the boundary midpoint, whereas the HP approach (filled, pink circle) generates £30.4k difference. The HP approach generates smaller absolute differences in arable costs for all coastal hazard uncertainty conditions. Both events show steep trends indicating increased uncertainty in boundary condition increases sensitivity of arable land costs. Both events also show sensitivity to approach to forcing the model boundary, indicated by the large differences between WR and HP symbols. Sensitivity to approach to forcing the model boundary may also be caused by the land types that are inundated close to flood pathways.

Figure 9b shows absolute difference in suburban costs compared to run 8. Wider spacing between the WR and HP symbols for the more extreme January 14 event indicates greater sensitivity to boundary forcing approach. For run 1 using the WR approach £27.9 M difference in suburban costs is generated, whereas the HP approach generates £1.9 M difference; sensitivity to boundary forcing approach generates up to £25.9 M difference in suburban costs. Run 6 generates a 0.06 m difference in HP at the boundary for January 14, and still generates up to £12.4 M cost to suburbia. It is found crucial for shoreline management, infrastructure or residential planning to consider the sensitivity of flood damage costs to coastal hazard uncertainty for long term assessments. For both events WR generates greater difference in suburban costs, which may be due to suburban areas being more closely located to overwash and breach locations along the coastal defences and embankments. Further to this it can be expected that a more realistic model, such as the WR approach which considers surfzone and shoaling processes, gives a more accurate result and reliable representation of flood hazard compared to the HP approach imposed at the LW mark. Overall, there is a steeper gradient in response to coastal hazard uncertainty for the January 14, compared to December 12.

4. Discussion

Coastal hazard uncertainty, due to coupling and forcing processes in WL and H_s prediction from Delft3D, was propagated through the LISFLOOD-FP Oldbury model domain using the hazard proxy (WL + $\frac{1}{2}$ Hs) and wave runup [59] approach to the force the model boundary for two historic storm events, to assess and quantify the sensitivity of inundation to these changes. Impact proxies include inundation water volume, inundation maps (and extent of different percentage water depths), flood hazard rating at two specific locations (receptors) and economic cost of inundation across the model domain to compare cases. On the basis of this case study, it has been shown that flood hazard is sensitive to uncertainty in the hydrodynamic forcing and nearshore topography affecting the water

level, significant wave height, runup and subsequent inundation water volumes. Inundation shows greatest sensitivity to event severity, as the January 14 event consistently generated greatest impact of inundation, presented here as flood hazard rating, volume of floodwater and economic cost. Flood hazard is also sensitive to the hinterland topography which controls how the hazard spreads through the domain to impact specific receptors and surfaces.

The results show that optimal model setup should include local atmospheric forcing and two-way coupling; the modelled outputs from the Delft3D-FLOW-WAVE setup for run 8 was validated to tide gauges and wave buoys [25], and representative inundation when qualitatively compared to flood zones in Shoreline Management Plans for the Severn Estuary. A well validated model setup will generate more accurate HWH$_s$ and HWL predictions, realistic predictions of inundation and cost of damage. Excluding local atmospheric forcing could under predict urban damage by up to £26.2 M when considering flooding for long-term hazard assessments and emergency response planning. Excluding two-way coupling processes could cost £12.4 M in a flood damage assessment, and exclusion of both forcing and coupling processes could cost up to £60.3 M.

4.1. Flood Hazard Sensitivity to Coastal Hazard Conditions and Approach to Forcing the Model Boundary

LISFLOOD-FP confirms that run 8 (two-way coupling + local atmospheric forcing) generates the largest volume of inundation, 12.5 Mm^3 and greatest economic cost to arable (£4.31 M) and suburban (£60.91 M) land using the wave runup approach for January 14 event. For this event HWH$_s$ is 0.94 m, superimposed on HWL of 9.4 m. Larger waves during the more extreme coastal hazard condition at the time of tidal high water have a greater impact on wave runup, and contribute more directly as a source of flood hazard. A coupled wave-tide model applied to the Irish Sea has shown that wave-tide interaction can increase high water wave heights up to 20% in regions with larger tidal range [72]. Wave-tide interaction is extremely important within flood hazard assessments and must be accounted for in coastal hydrodynamic models to accurately generate the largest waves at high water, which have been shown here to generate the greatest physical and economic impacts of flooding.

4.1.1. Influence of Coastal Hazard Condition

Larger wave runup is generated for the January 14 event, which takes into consideration both significant wave height and peak wave period. A longer peak wave period at the time of the storm tide peak and higher significant wave height for the January 14 event means a larger wave runup is calculated. The steepness of the coastline also plays an important role in controlling the calculated wave runup. Steeper embankments in the northeast of the domain also contribute to a larger calculated wave runup, and act as a pathway for flood hazard during the LISFLOOD-FP simulation to increase inundation in Oldbury-on-Severn. The December 12 event generates substantially smaller time-integrated volume of inundation using both the hazard proxy and wave runup approach, as observation data from the Scarweather wave buoy shows this event has a HWH$_s$ of 0.31 m, superimposed on a HWL of 8.09 m recorded at Ilfracombe tide gauge.

Smaller waves and shorter wave period for December 12 event means that smaller wave runup is generated and no flood pathway over the earthen embankments is created for the wave runup approach, and hazard thresholds are not exceeded for the hazard proxy approach. Event severity has been shown to be an important control on flood hazard in hyper-tidal estuaries [5], as higher water levels during extreme events can propagate wave energy shoreward [73].

Larger wave runup superimposed on a large spring tide, exacerbated in the northwest of the domain due to steeper embankments, represents a source of hazard, and creates multiple flood pathways (routes for the water to take) into the model domain [74]. The wave runup approach generates more inundation behind steep earthen embankments due to overwash of greenwater, in addition to inundation in the towns of Berkeley and Oldbury-on-Severn (see Figure 5). Once critical thresholds have been exceeded, the wave runup approach further exacerbates flood hazard as the boundary is located on the defence crest; the model domain has less floodwater accomodation so

floodwater is 'locked in'; there is no intertidal space in the model domain for floodwater to gravity drain into through the rhines and channels after HW. High 'tail water' conditions from a flood tide or storm surge have been shown to prevent drainage, and can exacerbate other flooding source-receptor pathways (e.g., flooding due to wave overwashing and defence breaching) [74,75]. Here we show that more extreme storm events and local, site-specific morphology of the coastline generates larger wave runup and more overwashing, to increase flood hazard. The wave runup approach increases the volume of inundation as floodwater enters the domain at multiple locations, and is retained in the model domain which generates an additional compound flooding pathway. The research has shown that different sources of uncertainty can combine with each other to increase uncertainty in flood hazard inundation. The relative importance of each source of uncertainty in flood hazard can vary through the course of the inundation simulation (e.g., event severity durng the flood stage, boundary forcing approach during the ebb stage).

4.1.2. Influence of Approach to Forcing the Model Boundary

Flood hazard is also sensitive to event severity and local morphology of the coastline using the hazard proxy approach. Run 8, used throughout as the baseline, for the 3 January 2014 event generates 2.5 Mm^3/s time-integrated volume of inundation using the hazard proxy approach for run 8, compared to 4.7 Mm^3/s generated from the wave runup approach. The position of the boundary using the hazard proxy approach means there is greater floodwater accommodation to provide space for floodwater to drain into in the intertidal areas, unlike the wave runup approach. This shows that boundary position alters the flood hazard within the model domain, by providing floodwater accommodation and easier drainage pathways on the ebb tide. The influence and importance of uncertainty of input factors on flood hazard sensitivity can change over the course of a flood event; it has been shown that the rising limb of an inflow hydrograph is most important during the flood stage of inundation in the coastal city of Licata, Sicily, then the channel friction parameter is most impotant during peak inundation and floodplain friction parameter during drying phase of the flood [31].

The results presented here show the combined effect of extra- and intra-model uncertainties [34] on flood hazard. Extra-model uncertainties relate to the data and approaches used to force the model boundary. Accurate total water level and wave predictions are important for assessing flood risk in coastal areas with high tidal ranges, or subject to large storm surges [76]. However, model sensitivities vary across space and the contribution of each physical process to a compound flooding pathway is site specific. For example, larger water levels are more important than wave height for inundation for storm events with a 0.5% probability in Dungeness, UK, as 5.28 m WL + 0.92 m H$_s$ will cause more inundation than 1.8 m WL and 5.72 m H$_s$ [77]. Intra-model uncertainties, such as boundary position or model domain size, influences floodwater pathways and controls the simulated spatial pattern of inundation and retention of flood water. This research shows changing the approach to boundary forcing influences the flooding pathways and drainage of floodwater at a local scale. The wave runup approach is the more sophisticated approach, as it considers how surfzone and shoaling effects transform deep water waves to the coastline, and generates £11.8 M less subsequent damage costs for suburbia when comparing run 1 for each approach. Structures within the model domain, e.g., the position of bridges, can influence the amount of backwater held in a modelled region to influence flood hazard [78], in addition to uncertainty in upstream boundary conditions. The spatial resolution of the DEM may contribute to uncertainty, but is not influential during the wetting phase of large storm events as the rapid rising limb indicates floodwaters are deep enough to move across small fluctuations in topography, but may be more influential during the recession of floodwaters or for less severe events [31]. It may also be important to include infiltration coefficients and groundwater flow to represent drainage more accurately through the model domain. The causes of sensitivity in inundation models interact with each other [79], and each input factor will require more or less consideration dependent on the decisions or assessments the inundation model is being used to support, or the scale of the area being considered.

4.2. Flood Hazard Sensitivity in Coastal Zones Worldwide

The model illustrates that flood hazard is sensitive to coastal hazard uncertainty, as the inclusion of local atmospheric forcing or coupling processes influences the impacts of flooding. Sensitivity of inundation to boundary conditions has been shown in studies worldwide. Uncertainty in boundary forcing, due to interpolation of boundary conditions in data poor regions, has been shown to generate greater uncertainty within an inundation model compared to DEM uncertainty when simulating future storm tide conditions in the Bay of Bengal [68]. Different approaches to generating boundary conditions for LISFLOOD-FP (e.g., based on linear interpolation of extreme values, or spatial characteristics of observed storm tides) caused up to 90 cm difference in storm tide peak along the North Somerset coastline, UK when simulating inundation from the December 13 1981, and subsequently up to 8.9 km^2 difference in overall inundation [66]. Uncertainty in coastal water levels and defence failures have been shown to generate greatest sensitivity in coastal flooding of Canvey Island, UK, as opposed to model terrain and bottom friction [80]. A water level elevation error of 2–3 cm, due to error in observation of tidal level or lack of wave forcing, has been shown to generate 3–25% variation in flood area in Newport Beach, California, dependent on location and hydraulic connectivity [81]. Flood inundation simulations are sensitive to the choice and design of boundary conditions, and it is important to accurately capture the hydrodynamic and atmospheric conditions occurring during extreme events [36] for storm hazard mitigation, adaptation and resilience planning. Large uncertainties in the hydrodynamic forcing of process-based and shoreline response models can have substantial practical and financial impacts, as the outputs from these models are used to understand extent and pathways of floodwater to guide decisions about the design and location of sea defences and coastal development, assess options for flood prevention schemes and prioritise areas which would benefit from adaptation and mitigation strategies [82–84].

The model shows that for all runs, once conditions exceed hazard thresholds to cause coastal flooding then even small changes in coastal hazard uncertainty matter in terms of the cost of flood damages. A 0.45 cm difference in coastal hazard uncertainty at the boundary using the wave runup approach for the January 14 event can cause up to 2.82 Mm^3/s difference in time-integrated volume of inundation and £27.9 M difference in economic cost to suburban land. Even as small a change in hazard proxy at the boundary as 0.06 m can generate up to 0.8 Mm^3/s difference in time-integrated volume of inundation, and £12.4 M difference in cost to suburban land. The error arising from coastal hazard uncertainty (up to 0.45 m) is greater than error that may be introduced into model simulations by the vertical accuracy of the DEM (0.05–0.15 m) or the wave runup formula (0.28–0.36 m) [85].

4.3. Implications for Inundation under Future Sea-Level Scenarios

The Severn Estuary is likely to experience increased flood hazard and inundation under future sea-level rise, with 2% probability of flooding near Berkeley-on-Severn, 1% near Littleton-upon-Severn, and up to 20% probability in low-lying agricultural areas near Shepperdine, east of Oldbury Technical Centre [63]. Flood hazard could increase by 29.7% under future extreme sea-level rise [32,33], indicating there is a need to plan for these changes for resilience and adaptation strategies in the estuary.

Small changes in coastal hazard uncertainty, due to forcing and coupling processes in the boundary conditions, can enlarge flooded areas and increase damage costs, and the methodology could be used to evaluation the impact of future sea-level rise in coastal and estuarine areas. The changes in total water level at the coastline presented here are within the range of the Intergovernmental Panel on Climate Change (IPCC) global projections of SLR, which range from 28 to 98 cm by 2100 [86] and the UKCP18 projections in Cardiff range from 0.27 to 1.31 m by 2100 [87]. Even a small change in sea-level rise will have a large impact on flood hazard as tidal amplitudes and estuarine morphologies change [88], and compound flood pathways may be exacerbated [89]. As the baseline on which storm surges and waves act is raised, wave energy propagates further shoreward exposing communities and infrastructure to the increased probability of defence failure [90,91]. Many low-lying areas that are

sensitive to coastal flooding during storm events will be overwhelmed with just 25 cm of sea-level rise along the California coastline; in combination with a 1:100 year storm event this could cause substantial flooding that would impact 150,000 residents and cause up to $30 billion damage [92]. Future sea-level rise will increase 'tail waters' and reduce the rate at which low-lying coastal and estuarine areas are able to drain floodwater, increasing the likelihood of further inundation from subsequent storm or rainfall events [93]. Extreme events can cause initial damage from flooding, but lack of drainage, potentially exacerbated by subsequent events, can cause knock-on effects to impact economic sectors in relation to closure of ports and harbours or disruption of transport of goods, and critical services (e.g., power, water, and communications), essential for public safety. However, the response of estuarine areas to sea-level rise threats may be dependent on their size, as large estuaries may experience increased channel volume due to sediment starvation, and subsequently flood hazard may be reduced [88]. Flood hazard assessments should, of course, be site-specific and targeted at understanding local or regional conditions under changing climate conditions, which can provide information on impacts in local areas of high flood risk. Inundation studies can support targeted adaptation strategies, allow coastal authorities to warn people living in high risk areas, and reduce risk by implementing resilience measures to minimise flood depths or improve drainage.

4.4. Limitations

The sensitivity of flood inundation to coastal hazard conditions due to the setup of the regional model and approach to force the model boundary are shown at Oldbury-on-Severn, southwest England. The boundary conditions used to force LISFLOOD-FP are derived from water level and significant wave height simulations in Delft3D. These simulations have been successfully validated to five tide gauges and four wave buoys within the Severn Estuary, southwest England, and south Wales. However, the lack of available data makes calibration and validation of an inundation more challenging than a hydrodynamic model. The January 14 event presented here resulted in inundation in the upper Severn Estuary, and this is well documented in media sources and local authority reports [94]. Shoreline Management Plans and Government flood maps for planning can also be used to assess identify known areas of risk that are likely to flood. These resources are valuable in qualitatively assessing floodwater routing, and where inundation occurred. Information that would aid validation of the modelled outputs, including the routing of floodwater, defence failure, inland extents of inundation, and cost of damage are not available. This qualitative assessment is a common approach [66]. Observed water levels from satellite images [95], or from debris lines left by receding waters [96] have been successfully used for validation purposes; however, this method is also dependent on data availability. Comparison of the results presented here with actual damage costs is also challenging; information on local scale impacts on arable land uses is not made available by land owners. Further to this, the depth damage curves used here do not consider the cost of damage due to wave processes or structure type and provide an indication of potential cost due to specific coastal hazard conditions for two land uses. Therefore, the inundation extent simulated by run 8 for January 14 and December 12 and cost of damage may not match that observed. Nevertheless, the differences in hazard proxies between each simulation is assumed to represent the uncertainty of inundation due to setup of the regional model and approach to force the boundary, which can inform and improve the accuracy of future, local flood hazard assessments.

The approaches to forcing the model boundary represent two proxies used by managers for estimating wave impacts at the coast. Calculating hazard proxy and wave runup are two tools available to transform offshore information from regional models, and are used here as an indicator of how waves may overwash defences at the coast. Water level + wave runup is a dynamic and intermittent process, with a latency in the order of seconds. Wave runup is applied here with the 15-min time step of water level and wave height outputs from Delft3D. This is a common approach, however larger significant wave height or longer wave periods which may be simulated at a finer temporal resolution may underestimate wave runup, particularly in regions of the model domain with steeper

slopes. Wave overwashing or overtopping volumes and discharges could be calculated as hazard estimators and applied to force the model boundary of inundation models [37]. The methodology shown here is applied to the Severn Estuary as an example of the sensitivity of flood hazard to coastal hazard conditions and approach to force the model boundary in a hyper-tidal estuary. This estuary is tide-dominant with a relatively low wave environment due to its shape, size and length scale [97]. The methodology could be applied to other estuaries worldwide, where the components of inundation will vary due to the individual shape and size of each system.

5. Conclusions

The combined effect of astronomical tides, meteorological storm surges, wind and waves can increase flood hazard in heavily populated and industrialised estuaries, which are the focal point of coastal megacities, critical infrastructure and economic activity. Accurate predictions of high water level and high water significant wave height are required to develop hazard maps or warning systems to mitigate the negative effects of combined flood hazards. However, uncertainties in high water level and high water significant wave height predictions can propagate through the modeling chain to cause uncertainties in process-based and shoreline response models, which are used to support decisions for storm hazard mitigation.

Time- and space-varying predicted water level and significant wave height at the coast from eight Delft3D-FLOW-WAVE model simulations, each representing uncertainty due to coupling and forcing processes, force LISFLOOD-FP, a 2D inundation model, at Oldbury-on-Severn, southwest England. Two approaches to forcing the model boundary were used; hazard proxy was imposed at the low water mark, and wave runup combined with water level at the defence crest. Simulations were completed for 3 January 2014 event, representing the most extreme coastal hazard condition on record, and 16 December 2012 representing the 90th percentile coastal hazard condition. Inundation is sensitive to sources of flood hazard, notably coastal hazard condition and coastal hazard uncertainty. The 3 January 2014 event generates the greatest impact of inundation, as larger high water level and high water wave height increases the peak and width of wave runup and hazard proxy. Run 8 generates up to 12.5 Mm^3 of flood water and £60.9 M cost of damage to suburban land using the wave runup approach, caused by overwashing of greenwater at the defence. Once the conditions in run 8 exceed the hazard thresholds to cause coastal flooding, then small changes in the condition matter in terms of the cost of flood damages. It is extremely important for flood hazard assessments to account for wave-tide interaction, which can increase high water significant wave height in numerical model predictions and will propagate through the modelling chain to influence the magnitude of flooding impacts.

The inclusion of local atmospheric forcing is important for reducing uncertainty in inundation, and coupling processes can help improve accuracy. This is confirmed by results from run 6, which simulates inundation most closely with run 8 (used here as the baseline), and generates smallest changes in flood hazard rating, time-integrated volume of inundation and economic costs compared to run 8. Further to this, run 3 and 4 generate up to 4.7 Mm^3/s difference in time-integrated volume of inundation run 8, as they are forced with a constant water level; total water level is unrealistic and greatly underestimated when tide is not included as a physical forcing process at the boundary. The exclusion of local atmospheric forcing could under-predict damage by £26.2 M when considering flooding for long-term, shoreline management plans. Coastal hazard uncertainty also has implications for emergency response planning, as events can present a danger to all or to none.

Impacts of inundation are also sensitive to approach to forcing the model boundary, which interacts with coastal hazard condition to alter the pathway of flood hazard. Once the threshold for flooding is exceeded compound flood pathways can be exacerbated due to coastal hazard condition and approach used to force the model boundary during the flood phase, as site-specific morphology of the coastline increases peak wave runup and location of overwash, and floodwater accommodation in the model domain influences drainage after the peak of the flood. The results show that even a small change

in coastal hazard uncertainty of 0.06 m, representing the change in total water level used to force the boundary of LISFLOOD-FP, can influence peak hazard proxy and wave runup and locations of overwash to cause up to 97.7 Mm^3 difference in time-integrated volume of inundation and £12.4 M difference in cost of damage to suburban land. These small changes in total water level at the boundary can be used to infer how small changes in future sea level could have a large impact on coastal inundation. Contributions to uncertainty in inundation models should be considered when developing local scale studies of storm events under present and future sea-level scenarios for storm hazard mitigation and adaptation or resilience planning.

Supplementary Materials: The following are available online at http://www.mdpi.com/2077-1312/8/9/724/s1, Figure S1: Depth and extent of flooding at Oldbury-on-Severn for HP approach to forcing the model boundary where maps 1-8 represent coastal hazard uncertainty (see Table 1) for December 12, Figure S2: Depth and extent of flooding at Oldbury-on-Severn for WR approach to forcing the model boundary where maps 1-8 represent coastal hazard uncertainty (see Table 1) for December 12, Table S1: Water depth percentiles for January 14 WR, Table S2: Water depth percentiles for January 14 HP, Table S3: Water depth percentiles for December 12 WR, Table S4: Water depth percentiles for December 12 HP.

Author Contributions: Conceptualization, C.E.L.; Formal analysis, C.E.L.; Investigation, C.E.L.; Methodology, C.E.L.; Supervision, J.M.B., N.L. and A.J.P.; Validation, C.E.L.; Visualization, C.E.L., J.M.B., N.L. and A.J.P.; Writing—original draft, C.E.L.; Writing—review & editing, J.M.B., N.L. and A.J.P. All authors have read and agreed to the published version of the manuscript.

Conflicts of Interest: The authors declare no conflict of interest.

References

1. Adikari, Y.; Osti, R.; Noro, T. Flood-related disaster vulnerability: An impending crisis of megacities in Asia. *J. Flood Risk Manag.* **2010**, *3*, 185–191. [CrossRef]
2. Sekovski, I.; Newton, A.; Dennison, W.C. Megacities in the coastal zone: Using a driver-pressure-state-impact-response framework to address complex environmental problems. *Estuar. Coast. Shelf Sci.* **2012**, *96*, 48–59. [CrossRef]
3. Chen, R.; Zhang, Y.; Xu, D.; Liu, M. Climate change and coastal megacities: Disaster risk assessment and responses in Shanghai City. In *Climate Change, Extreme Events and Disaster Risk Reduction*; Springer Science and Business Media LLC: Berlin, Germany, 2017; pp. 203–216.
4. Hendry, A.; Haigh, I.D.; Nicholls, R.J.; Winter, H.; Neal, R.; Wahl, T.; Joly-Laugel, A.; Darby, S.E. Assessing the characteristics and drivers of compound flooding events around the UK coast. *Hydrol. Earth Syst. Sci.* **2019**, *23*, 3117–3139. [CrossRef]
5. Lyddon, C.; Brown, J.M.; Leonardi, N.; Plater, A.J. Flood hazard assessment for a hyper-tidal estuary as a function of tide-surge-morphology interaction. *Chesap. Sci.* **2018**, *41*, 1565–1586. [CrossRef]
6. Narayan, S.; Hanson, S.; Nicholls, R.J.; Clarke, D.; Willems, P.; Ntegeka, V.; Monbaliu, J. A holistic model for coastal flooding using system diagrams and the Source-Pathway-Receptor (SPR) concept. *Nat. Hazards Earth Syst. Sci.* **2012**, *12*, 1431–1439. [CrossRef]
7. Desplanque, C.; Mossman, D.J. Storm tides of the Fundy. *Geogr. Rev.* **1999**, *89*, 23–33. [CrossRef]
8. Greenberg, D.; Blanchard, W.; Smith, B.; Barrow, E. Climate change, mean sea level and high tides in the bay of Fundy. *Atmos. Ocean.* **2012**, *50*, 261–276. [CrossRef]
9. Muchan, K.; Lewis, M.; Hannaford, J.; Parry, S. The winter storms of 2013/2014 in the UK: Hydrological responses and impacts. *Weather* **2015**, *70*, 55–61. [CrossRef]

10. Sibley, A.; Cox, D.; Titley, H. Coastal flooding in England and Wales from Atlantic and North Sea storms during the 2013/2014 winter. *Weather* **2015**, *70*, 62–70. [CrossRef]

11. Yang, J.; Li, L.; Zhao, K.; Wang, P.; Wang, D.; Sou, I.M.; Yang, Z.; Hu, J.; Tang, X.; Mok, K.M.; et al. A comparative study of typhoon Hato (2017) and typhoon Mangkhut (2018)—Their Impacts on coastal inundation in Macau. *J. Geophys. Res. Ocean.* **2019**, *124*, 9590–9619. [CrossRef]

12. Haigh, I.D.; Wadey, M.P.; Wahl, T.; Ozsoy, O.; Nicholls, R.J.; Brown, J.M.; Horsburgh, K.; Gouldby, B. Spatial and temporal analysis of extreme sea level and storm surge events around the coastline of the UK. *Sci. Data* **2016**, *3*, 160107. [CrossRef] [PubMed]

13. Del Río, L.; Plomaritis, T.; Benavente, J.; Valladares, M.; Ribera, P.; González, J.B. Establishing storm thresholds for the Spanish Gulf of Cádiz coast. *Geomorphology* **2012**, *144*, 13–23. [CrossRef]

14. Teng, J.; Jakeman, A.; Vaze, J.; Croke, B.; Dutta, D.; Kim, S. Flood inundation modelling: A review of methods, recent advances and uncertainty analysis. *Env. Model. Softw.* **2017**, *90*, 201–216. [CrossRef]

15. Sénéchal, N.; Coco, G.; Bryan, K.R.; Holman, R.A. Wave runup during extreme storm conditions. *J. Geophys. Res. Space Phys.* **2011**, *116*, 7. [CrossRef]

16. Suanez, S.; Cancouët, R.; Floc'H, F.; Blaise, E.; Ardhuin, F.; Filipot, J.-F.; Cariolet, J.-M.; Delacourt, C. Observations and predictions of wave runup, extreme water levels, and medium-term dune erosion during storm conditions. *J. Mar. Sci. Eng.* **2015**, *3*, 674–698. [CrossRef]

17. EurOtop. *Manual on Wave Overtopping of Sea Defences and Related Structures*, 2nd ed.; Boyens Medien GmbH: Heide, Germany, 2018.

18. Knight, P.J.; Prime, T.; Brown, J.M.; Morrissey, K.; Plater, A.J. Application of flood risk modelling in a web-based geospatial decision support tool for coastal adaptation to climate change. *Nat. Hazards Earth Syst. Sci.* **2015**, *15*, 1457–1471. [CrossRef]

19. Prime, T.; Brown, J.M.; Plater, A.J. Physical and economic impacts of sea-level rise and low probability flooding events on coastal communities. *PLoS ONE* **2015**, *10*, e0117030. [CrossRef]

20. Didier, D.; Baudry, J.; Bernatchez, P.; Dumont, D.; Sadegh, M.; Bismuth, E.; Bandet, M.; Dugas, S.; Sévigny, C. Multihazard simulation for coastal flood mapping: Bathtub versus numerical modelling in an open estuary, Eastern Canada. *J. Flood Risk Manag.* **2018**, *12*, e12505. [CrossRef]

21. Thompson, D.A.; Karunarathna, H.U.; Reeve, D.E. Modelling extreme wave overtopping at aberystwyth promenade. *Water* **2017**, *9*, 663. [CrossRef]

22. Karunarathna, H.U.; Brown, J.M.; Chatzirodou, A.; Dissanayake, P.; Wisse, P. Multi-timescale morphological modelling of a dune-fronted sandy beach. *Coast. Eng.* **2018**, *136*, 161–171. [CrossRef]

23. Vitousek, S.; Barnard, P.; Fletcher, C.H.; Frazer, L.N.; Erikson, L.; Storlazzi, C.D. Doubling of coastal flooding frequency within decades due to sea-level rise. *Sci. Rep.* **2017**, *7*, 1399. [CrossRef] [PubMed]

24. DEFRA. Flood Risks to People (Phase 2). Flood Risks to People Phase 2 FD2321 Tech Rep 1 [Internet]. 2003; p. 117. Available online: http://randd.defra.gov.uk/Document.aspx?Document=FD2317_1060_TRP.pdf (accessed on 22 January 2020).

25. Amante, C. Estimating coastal digital elevation model uncertainty. *J. Coast. Res.* **2018**, *34*, 1382–1397. [CrossRef]

26. Lyddon, C.E.; Brown, J.M.; Leonardi, N.; Saulter, A. Quantification of the uncertainty in coastal storm hazard predictions due to wave—Current interaction and wind forcing. *Geophys Res Lett.* **2019**, *46*, 14576–14585. [CrossRef]

27. Stephens, S.A.; Bell, R.; Lawrence, J. Applying principles of uncertainty within coastal hazard assessments to better support coastal adaptation. *J. Mar. Sci. Eng.* **2017**, *5*, 40. [CrossRef]

28. Sayers, P.; Gouldby, B.; Simm, J.; Meadowcroft, I.; Hall, J. Risk, performance and uncertainty in flood and coastal defence—A review. *R&D Tech. Rep.* **2003**, *115*, 6–27.

29. Hewston, R.; Zou, Q.; Reeve, D.; Pan, S.; Chen, Y. Quantifying uncertainty in tide, surge and wave modelling during extreme storms. In Proceedings of the BHS 3rd International Symposium, Managing Consequences of Changing Global Environment, British Hydrological Society, Newcastle University, Newcastle, UK, 19–23 July 2010.

30. Kumbier, K.; Carvalho, R.C.; Vafeidis, A.T.; Woodroffe, C.D. Investigating compound flooding in an estuary using hydrodynamic modelling: A case study from the Shoalhaven River, Australia. *Nat. Hazards Earth Syst. Sci.* **2018**, *18*, 463–477. [CrossRef]

31. Savage, J.T.S.; Pianosi, F.; Bates, P.D.; Freer, J.E.; Wagener, T. Quantifying the importance of spatial resolution and other factors through global sensitivity analysis of a flood inundation model. *Water Resour. Res.* **2016**, *52*, 9146–9163. [CrossRef]

32. Purvis, M.J.; Bates, P.D.; Hayes, C.M. A probabilistic methodology to estimate future coastal flood risk due to sea level rise. *Coast. Eng.* **2008**, *55*, 1062–1073. [CrossRef]

33. Quinn, N.; Bates, P.D.; Siddall, M. The contribution to future flood risk in the Severn Estuary from extreme sea level rise due to ice sheet mass loss. *J. Geophys. Res. Ocean.* **2013**, *118*, 5887–5898. [CrossRef]

34. Lewis, M.J.; Schumann, G.J.-P.; Bates, P.D.; Horsburgh, K. Understanding the variability of an extreme storm tide along a coastline. *Estuar. Coast. Shelf Sci.* **2013**, *123*, 19–25. [CrossRef]

35. Pianosi, F.; Beven, K.; Freer, J.E.; Hall, J.W.; Rougier, J.; Stephenson, D.; Wagener, T. Sensitivity analysis of environmental models: A systematic review with practical workflow. *Env. Model. Softw.* **2016**, *79*, 214–232. [CrossRef]

36. Pasquier, U.; He, Y.; Hooton, S.; Goulden, M.; Hiscock, K.M. An integrated 1D–2D hydraulic modelling approach to assess the sensitivity of a coastal region to compound flooding hazard under climate change. *Nat. Hazards* **2018**, *98*, 915–937. [CrossRef]

37. Sanuy, M.; Jimenez, J.A.; Ortego, M.I.; Toimil, A. Differences in assigning probabilities to coastal inundation hazard estimators: Event versus response approaches. *J. Flood Risk Manag.* **2019**, *13*, 7. [CrossRef]

38. Hall, J.W.; Solomatine, D. A framework for uncertainty analysis in flood risk management decisions. *Int. J. River Basin Manag.* **2008**, *6*, 85–98. [CrossRef]

39. SurgeWatch. An Interactive Database of UK Coastal Flooding [Internet]. 2018. Available online: https://www.surgewatch.org/ (accessed on 11 July 2020).

40. Haigh, I.D.; Wadey, M.P.; Gallop, S.L.; Loehr, H.; Nicholls, R.J.; Horsburgh, K.; Brown, J.M.; Bradshaw, E. A user-friendly database of coastal flooding in the United Kingdom from 1915–2014. *Sci. Data* **2015**, *2*, 150021. [CrossRef]

41. Uncles, R. Physical properties and processes in the Bristol Channel and Severn Estuary. *Mar. Pollut. Bull.* **2010**, *61*, 5–20. Available online: http://linkinghub.elsevier.com/retrieve/pii/S0025326X09005128 (accessed on 21 January 2020). [CrossRef]

42. Pye, K.; Blott, S.J. A consideration of "extreme events" at Hinkley Point. *Tech. Rep. Ser.* **2010**, *2010*, 109.

43. JBA. South Gloucestershire Council Strategic Flood Risk Assessment Level 2 for Oldbury on Severn JBA Project Manager. 2017. Available online: https://beta.southglos.gov.uk/wp-content/uploads/South-Gloucestershire-Council-level-2-Strategic-Flood-Risk-Assessment-SFRA-for-Oldbury-on-Severn-Sept-2017.pdf (accessed on 10 July 2020).

44. South Gloucestershire Council. Southampton Local Flood Risk Management Strategy Summary [Internet]. 2014. Available online: https://www.southampton.gov.uk/policies/SouthamptonLFRMSMainReport--Final-October2014.pdf (accessed on 10 July 2020).

45. Office for National Statistics. Oldbury, Berkeley and Thornbury parish [Internet]. 2011. Available online: https://www.nomisweb.co.uk/ (accessed on 20 April 2020).

46. Bates, P.D.; Dawson, R.J.; Hall, J.W.; Horritt, M.S.; Nicholls, R.J.; Wicks, J.; Hassan, M.A.A.M. Simplified two-dimensional numerical modelling of coastal flooding and example applications. *Coast. Eng.* **2005**, *52*, 793–810. [CrossRef]

47. Wadey, M.P.; Nicholls, R.J.; Hutton, C. Coastal flooding in the solent: An integrated analysis of defences and inundation. *Water* **2012**, *4*, 430–459. [CrossRef]

48. Skinner, C.; Coulthard, T.J.; Parsons, D.R.; Ramirez, J.; Mullen, L.; Manson, S. Simulating tidal and storm surge hydraulics with a simple 2D inertia based model, in the Humber Estuary, U.K. *Estuar. Coast. Shelf Sci.* **2015**, *155*, 126–136. [CrossRef]

49. Smith, R.A.; Bates, P.D.; Hayes, C. Evaluation of a coastal flood inundation model using hard and soft data. *Env. Model. Softw.* **2011**, *30*, 35–46. [CrossRef]

50. Quinn, N.; Lewis, M.; Wadey, M.P.; Haigh, I.D. Assessing the temporal variability in extreme storm-tide time series for coastal flood risk assessment. *J. Geophys. Res. Ocean.* **2014**, *119*, 4983–4998. [CrossRef]

51. Environment Agency Geomatics. LiDAR Download [Internet]. Available online: https://www.arcgis.com/apps/MapJournal/index.html?appid=c6cef6cc642a48838d38e722ea8ccfee (accessed on 12 August 2019).

52. Seenath, A. Effects of DEM resolution on modeling coastal flood vulnerability. *Mar. Geod.* **2018**, *41*, 581–604. [CrossRef]

53. Md Ali, A.; Solomatine, D.P.; Di Baldassarre, G. Assessing the impact of different sources of topographic data on 1-D hydraulic modelling of floods. *Hydrol. Earth Syst. Sci.* **2015**, *19*, 631–643. [CrossRef]

54. Karamouz, M.; Fereshtehpour, M. Modeling DEM errors in coastal flood inundation and damages: A spatial nonstationary approach. *Water Resour. Res.* **2019**, *55*, 6606–6624. [CrossRef]

55. Saulter, A.; Bunney, C.; Li, J. *Application of a Refined Grid Global Model for Operational Wave Forecasting*; Met Office: Exeter, UK, 2016.

56. Siddorn, J.; Good, S.A.; Harris, C.M.; Lewis, H.W.; Maksymczuk, J.; Martin, M.J.; Saulter, A. Research priorities in support of ocean monitoring and forecasting at the Met Office. *Ocean Sci.* **2016**, *12*, 217–231. [CrossRef]

57. Walters, D.N.; Williams, K.D.; Boutle, I.A.; Bushell, A.C.; Edwards, J.; Field, P.R.; Lock, A.P.; Morcrette, C.J.; Stratton, R.A.; Wilkinson, J.; et al. The Met Office unified Model Global Atmosphere 4.0 and JULES Global Land 4.0 configurations. *Geosci. Model. Dev.* **2014**, *7*, 361–386. [CrossRef]

58. Williams, J.A.; Horsburgh, K.J.; Evaluation and comparison of the operational Bristol Channel Model storm surge suite. NOC Res. *Consult. Rep.* **2013**. Available online: http://nora.nerc.ac.uk/id/eprint/502138/1/NOC_R%26C_38.pdf (accessed on 21 January 2020).

59. Stockdon, H.F.; Holman, R.A.; Howd, P.A.; Sallenger, A.H. Empirical parameterization of setup, swash, and runup. *Coast. Eng.* **2006**, *53*, 573–588. [CrossRef]

60. Melby, J.; Nadal-Caraballo, N.; Kobayashi, N. Wave runup prediction for flood mapping. In Proceedings of the Coastal Engineering Proceedings; Coastal Engineering Research Council, Santander, Spain, 1–6 July 2012; Volume 1, pp. 1–15.

61. Severn Estuary Coastal Group. Severn Estuary Shoreline Management Plan: PART B – POLICY STATEMENTS [Internet]. 2016. Available online: https://www.slideshare.net/SevernEstuary1/smp2-part-b-policy-statements-intro-sectionsfinal (accessed on 11 July 2020).

62. Environment Agency. Flood Map for Planning [Internet]. 2020. Available online: https://flood-map-for-planning.service.gov.uk (accessed on 11 July 2020).

63. Environment Agency. Managing Flood Risk on the Severn Estuary [Internet]. 2011. Available online: http://severnriverstrust.com/ManagingFloodRiskontheSevernEstuary-SthGloucsHinkleyPointSomerset(Jan11).pdf (accessed on 11 July 2020).

64. Chow, V.T. *Open-Channel Hydraulics*; McGraw-Hill: New York, NY, USA, 1959; p. 680.

65. Ding, Y.; Jia, Y.; Wang, S.S.Y. Identification of manning's roughness coefficients in shallow water flows. *J. Hydraul. Eng.* **2004**, *130*, 501–510. [CrossRef]

66. Lewis, M.J.; Horsburgh, K.; Bates, P.D.; Smith, R. Quantifying the uncertainty in future coastal flood risk estimates for the U.K. *J. Coast. Res.* **2011**, *276*, 870–881. [CrossRef]

67. Brown, J.M.; Prime, T.; Phelps, J.J.; Barkwith, A.; Hurst, M.D.; Ellis, M.A.; Masselink, G.; Plater, A.J. Spatio-temporal variability in the tipping points of a coastal defense. *J. Coast. Res.* **2016**, *75*, 1042–1046. [CrossRef]

68. Lewis, M.J.; Bates, P.D.; Horsburgh, K.; Neal, J.; Schumann, G.J.-P.; Neal, J.C. A storm surge inundation model of the northern Bay of Bengal using publicly available data. *Q. J. R. Meteorol. Soc.* **2013**, *139*, 358–369. [CrossRef]

69. Bates, P.; Trigg, M.; Neal, J.; Dabrowa, A. *LISFLOOD-FP User Manual: Code Release 5.9.6*; University of Bristol: Bristol, UK, 2013.

70. Penning-Rowsell, E.; Priest, S.; Parker, D.; Morris, J. *Flood and Coastal Erosion Risk Management*; Informa UK Limited: Colchester, UK, 2014.

71. Rowland, C.S.; Morton, R.D.; Carrasco, L.; McShane, G.; O'Neil, A.W.; Wood, C.M. Land Cover Map 2015 (25m raster, GB) [Internet]. NERC Environmental Information Data Centre. 2017. Available online: https://doi.org/10.5285/bb15e200-9349-403c-bda9-b430093807c7 (accessed on 12 August 2019).

72. Lewis, M.J.; Palmer, T.; Hashemi, R.; Robins, P.; Saulter, A.; Brown, J.; Lewis, H.; Neill, S. Wave-tide interaction modulates nearshore wave height. *Ocean. Dyn.* **2019**, *69*, 367–384. [CrossRef]

73. Gallien, T.W.; Kalligeris, N.; Delisle, M.-P.; Tang, B.-X.; Lucey, J.T.D.; Winters, M.A. Coastal flood modeling challenges in defended urban backshores. *Geoscience* **2018**, *8*, 450. [CrossRef]

74. Gallien, T.; Sanders, B.; Flick, R. Urban coastal flood prediction: Integrating wave overtopping, flood defenses and drainage. *Coast. Eng.* **2014**, *91*, 18–28. [CrossRef]

75. Wahl, T.; Jain, S.; Bender, J.; Meyers, S.D.; Luther, M.E. Increasing risk of compound flooding from storm surge and rainfall for major US cities. *Nat. Clim. Chang.* **2015**, *5*, 1093–1097. [CrossRef]

76. Hawkes, P.J.; Gouldby, B.P.; Tawn, J.A.; Owen, M.W. The joint probability of waves and water levels in coastal engineering design. *J. Hydraul. Res.* **2002**, *40*, 241–251. [CrossRef]

77. Prime, T.; Brown, J.M.; Plater, A.J. Flood inundation uncertainty: The case of a 0.5% annual probability flood event. *Environ. Sci. Policy* **2016**, *59*, 1–9. [CrossRef]

78. Pappenberger, F.; Matgen, P.; Beven, K.J.; Henry, J.-B.; Pfister, L.; Fraipont, P. Influence of uncertain boundary conditions and model structure on flood inundation predictions. *Adv. Water Resour.* **2006**, *29*, 1430–1449. [CrossRef]

79. Perini, L.; Calabrese, L.; Salerno, G.; Ciavola, P.; Armaroli, C. Evaluation of coastal vulnerability to flooding: Comparison of two different methodologies adopted by the Emilia-Romagna region (Italy). *Nat. Hazards Earth Syst. Sci.* **2016**, *16*, 181–194. [CrossRef]

80. Brown, J.D.; Spencer, T.; Moeller, I. Modeling storm surge flooding of an urban area with particular reference to modeling uncertainties: A case study of Canvey Island, United Kingdom. *Water Resour. Res.* **2007**, *430*, 6. [CrossRef]

81. Gallien, T.; Schubert, J.E.; Sanders, B.F. Predicting tidal flooding of urbanized embayments: A modeling framework and data requirements. *Coast. Eng.* **2011**, *58*, 567–577. [CrossRef]

82. McLeod, E.; Poulter, B.; Hinkel, J.; Reyes, E.; Salm, R. Sea-level rise impact models and environmental conservation: A review of models and their applications. *Ocean. Coast. Manag.* **2010**, *53*, 507–517. [CrossRef]

83. SEPA. Flood Modelling Guidance for Responsible Authorities. 2018, p. 166. Available online: https://www.sepa.org.uk/media/219653/flood_model_guidance_v2.pdf (accessed on 12 July 2020).

84. Environment Agency. National Flood and Coastal Erosion Risk Management Strategy for England [Internet]. 2019. Available online: https://www.gov.uk/government/publications/national-flood-and-coastal-erosion-risk-management-strategy-for-england (accessed on 11 July 2020).

85. Stockdon, H.F.; Thompson, D.; Plant, N.G.; Long, J. Evaluation of wave runup predictions from numerical and parametric models. *Coast. Eng.* **2014**, *92*, 1–11. [CrossRef]

86. Church, J.A.; Clark, P.U.; Cazenave, A.; Gregory, J.; Jevrejeva, S.; Levermann, A.; Merrifield, M.A.; Milne, G.A.; Nerem, R.S.; Nunn, P.D.; et al. Sea-level rise by 2100. *Science* **2013**, *342*, 1445–1447. [CrossRef]

87. Lowe, J.A.; Bernie, D.; Bett, P.; Bricheno, L.; Brown, S.; Calvert, D.; Clark, R.; Eagle, K.; Edwards, T.; Fosser, G.; et al. UKCP18 Science Overview Report [Internet]. Vol. 2, Met Office. 2018. Available online: https://www.metoffice.gov.uk/pub/data/weather/uk/ukcp18/science-reports/UKCP18-Overview-report.pdf (accessed on 21 January 2020).

88. Leuven, J.R.F.W.; Pierik, H.J.; Van Der Vegt, M.; Bouma, T.J.; Kleinhans, M.G. Sea-level-rise-induced threats depend on the size of tide-influenced estuaries worldwide. *Nat. Clim. Chang.* **2019**, *9*, 986–992. [CrossRef]

89. Moftakhari, H.R.; Salvadori, G.; AghaKouchak, A.; Sanders, B.F.; Matthew, R.A. Compounding effects of sea level rise and fluvial flooding. *Proc. Natl. Acad. Sci. USA* **2017**, *114*, 9785–9790. [CrossRef]

90. Le Cozannet, G.; Rohmer, J.; Cazenave, A.; Idier, D.; Van De Wal, R.; De Winter, R.; Pedreros, R.; Balouin, Y.; Vinchon, C.; Oliveros, C. Evaluating uncertainties of future marine flooding occurrence as sea-level rises. *Environ. Model. Softw.* **2015**, *73*, 44–56. [CrossRef]

91. Marcos, M.; Rohmer, J.; Vousdoukas, M.I.; Mentaschi, L.; Le Cozannet, G.; Amores, A. Increased extreme coastal water levels due to the combined action of storm surges and wind waves. *Geophys. Res. Lett.* **2019**, *46*, 4356–4364. [CrossRef]

92. Barnard, P.; Erikson, L.; Foxgrover, A.C.; Hart, J.A.F.; Limber, P.; O'Neill, A.C.; Van Ormondt, M.; Vitousek, S.; Wood, N.J.; Hayden, M.K.; et al. Dynamic flood modeling essential to assess the coastal impacts of climate change. *Sci. Rep.* **2019**, *9*, 1–13. [CrossRef] [PubMed]

93. Amante, C. Uncertain seas: Probabilistic modeling of future coastal flood zones. *Int. J. Geogr. Inf. Sci.* **2019**, *33*, 2188–2217. [CrossRef]

94. Wales, N.R. Severn River Basin District. Consultation on the draft Flood Risk Management Plan. 2014. Available online: https://naturalresources.wales/media/682462/lit-10213_severn_frmp_part-a.pdf (accessed on 12 July 2020).

95. Mason, D.; Bates, P.; Dall' Amico, J.D. Calibration of uncertain flood inundation models using remotely sensed water levels. *J. Hydrol.* **2009**, *368*, 224–236. [CrossRef]

96. Wing, O.E.J.; Sampson, C.C.; Bates, P.D.; Quinn, N.; Smith, A.M.; Neal, J.C. A flood inundation forecast of Hurricane Harvey using a continental-scale 2D hydrodynamic model. *J. Hydrol. X* **2019**, *4*, 100039. [CrossRef]
97. Hume, T.M.; Snelder, T.; Weatherhead, M.; Liefting, R. A controlling factor approach to estuary classification. *Ocean. Coast. Manag.* **2007**, *50*, 905–929. [CrossRef]